CHAPTER

MULTICARRIER WAVEFORMS 5

The waveform is a core component of any communication technology. Broadly speaking, there are two main categories of waveforms: i) single-carrier waveforms, ii) multicarrier waveforms. 2G and 3G cellular systems (GSM, UMTS, CDMA2000) as well as ZigBee and Bluetooth adopted single-carrier waveforms. The 4G cellular system (LTE) employs a multicarrier waveform. Multicarrier waveforms are also used in asymmetric digital subscriber line (ADSL), wireless local area network (WLAN), WiMAX, digital audio broadcast (DAB), and digital video broadcast-terrestrial (DVB-T) standards. Typically, single-carrier waveforms have a low peak-to-average power ratio (PAPR), which makes them power efficient—suitable for coverage limited scenarios and extending battery life of user equipment. On the other hand, multicarrier waveforms provide high spectral efficiency, flexible resource allocation in the frequency domain, and possibly easy integration with multiantenna technology. These are the key drivers for 5G NR.

NR will support various use cases with different deployments in frequencies from below 1 GHz to 100 GHz. Although single-carrier waveforms can be interesting for massive IoT devices (with extended battery life) and for operation in high carrier frequencies (where transmission loss is high), the multicarrier waveforms have been seen as main candidates of 5G due to the reasons mentioned above. The 3GPP evaluated several multicarrier waveforms as well as single carrier waveforms. It was observed that different waveforms have their pros and cons, which makes different waveforms suitable in different scenarios. However, the 3GPP also acknowledged the fact that the 5G NR radio interface based on multiple waveforms will make the overall system design complex. Considering overall performance, system requirements, and the need for a single waveform, the 3GPP concluded in favor of OFDM for both uplink and downlink transmissions. Moreover, the DFT-Spread OFDM (DFTS-OFDM) waveform, which has single-carrier properties, has been kept as an option for uplink transmission in coverage limited scenarios.

This chapter presents various multicarrier waveforms and provides a comparison that has led to the down selection of OFDM for 5G NR. The chapter is structured as follows. Section 5.1 introduces state-of-the-art OFDM-based and filter bank multicarrier (FBMC)-based waveforms and Section 5.2 introduces the DFTS-OFDM waveform. Section 5.3 describes the waveform design requirements for NR. Section 5.4 presents the key indicators for waveform comparisons, based on which Section 5.5 compares performance of the multicarrier waveforms.

5.1 MULTICARRIER WAVEFORMS

The main principle behind multicarrier waveforms is to split a high rate data stream into multiple low rate streams that are transmitted simultaneously over a number of carriers (termed subcarriers). By doing so, the symbol duration for each low rate subcarrier increases and therefore the relative amount of time dispersion caused by a multipath (frequency selective) channel decreases. This makes

5G Physical Layer. https://doi.org/10.1016/B978-0-12-814578-4.00010-2

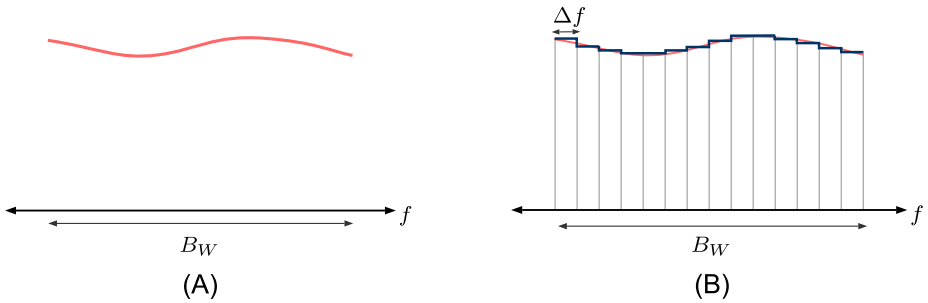

FIGURE 5.1

(A) Frequency-selective channel. (B) Frequency flat subchannels.

a multicarrier waveform robust to the intersymbol interference caused by the multipath channel. Let us look at this in the frequency domain. A frequency-selective fading channel is split into multiple (approximately) frequency flat channels and each subcarrier now experiences frequency flat fading, as illustrated in Fig. 5.1. This avoids complex time domain equalization, making the multicarrier transmissions suitable for high data rate wireless communication.

Multicarrier waveforms provide the freedom of multiplexing multiple users in the frequency domain (allocating different subcarriers to different users) and spatial domain (mapping different subcarriers to different antennas). Furthermore, multicarrier waveforms are robust to narrowband interference compared to single-carrier waveforms. In a multicarrier system, narrowband interference only corrupts a small number of subcarriers, whereas in a single-carrier transmission an entire link can fail due to narrowband interference.

5.1.1 THE PRINCIPLE OF ORTHOGONALITY

Mathematically, a multicarrier waveform in baseband can be expressed as

$$\widetilde{x}(t) = \sum_{s\in\mathbb{Z}} \sum_{i\in I} X_{s,i}\, \widetilde{p}_i(t - sT), \tag{5.1}$$

where s denotes the waveform symbol index, $\mathbb{Z}$ is a set of integers, i denotes the subcarrier index, $I \in \{i = 1, 2, \ldots, N\}$ contains indices of the subcarriers, N is the total number of subcarriers, $X_{i,s} \in \mathbb{C}$ is a complex modulated (QAM or phase shift keying (PSK)) symbol mapped to the subcarrier i and the symbol index s, and $\widetilde{p}_i(t)$ is a pulse shape (or prototype filter) used for the subcarrier i. Typically, $\widetilde{p}_i(t)$ is a bandpass filter centered at the subcarrier frequency f_i. For example, for OFDM, $\widetilde{p}_i(t) = \mathrm{e}^{j2\pi f_i t}$ for $0 \le t \le T$ and $\widetilde{p}_i(t) = 0$ elsewhere. In a multicarrier system, the number of active subcarriers is usually chosen smaller than the total number of subcarriers to relax filtering operations, i.e., $X_{i,s} = 0$ for some i at the band edges. The modulation and demodulation operations for a multicarrier system are illustrated in Fig. 5.2.

The demodulation operation is based on matched filtering, which is optimal for linear and additive noise channels in the sense of maximizing signal-to-noise ratio (SNR) of the demodulated (reconstructed) signal. The matched filter demodulation comprises the convolution of the received signal $\widetilde{r}(t)$

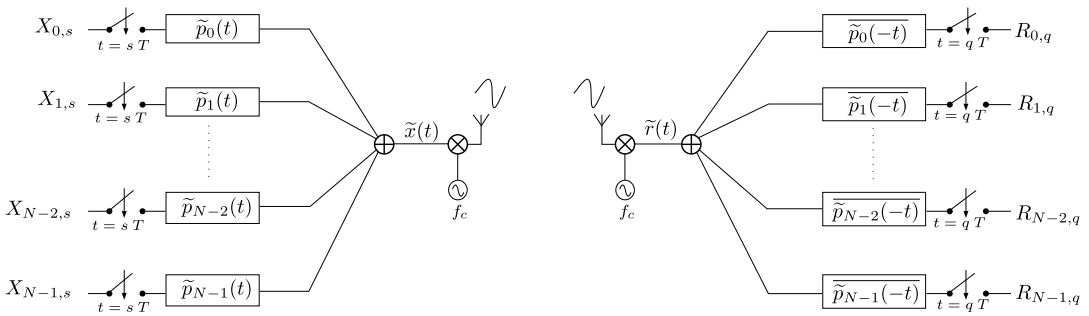

FIGURE 5.2

Modulation and demodulation process in a multicarrier system.

with the complex conjugated time-reversed version of the transmitter prototype filter (or pulse shape), followed by sampling at a rate equal to $\frac{1}{T}$. For simplicity, let us assume that $\widetilde{r}(t) = \widetilde{x}(t)$ and denote $R_{l,q}$ as demodulated (reconstructed) QAM (or PSK) symbol from a waveform symbol q and a subcarrier l. The demodulation operation is then given by

$$\begin{aligned} R_{l,q} &= \widetilde{r}(t) * \overline{\widetilde{p}_l(-t)}\Big|_{t=qT} \\ &\overset{(a)}{=} \left\langle \widetilde{r}(t), \widetilde{p}_l(t - qT) \right\rangle \\ &\overset{(b)}{=} \sum_{s\in\mathbb{Z}} \sum_{i\in I} X_{s,i} \left\langle \widetilde{p}_i(t - sT), \widetilde{p}_l(t - qT) \right\rangle, \end{aligned} \tag{5.2}$$

where $\overline{\widetilde{p}_i(t)}$ denotes complex conjugation of $\widetilde{p}_i(t)$; $*$ is the convolution operator; $\langle v_1(t), v_2(t)\rangle := \int_{\infty}^{\infty} v_1(t) v_2{}^*(t) dt$ denotes the inner product between $v_1(t)$ and $v_2(t)$; (a) follows from the definition of the convolution operation (i.e., expressing convolution in terms of correlation); and (b) follows from the assumption that $\widetilde{r}(t) = \widetilde{x}(t)$. From (5.2), we can see that the perfect reconstruction of the transmitted QAM symbols ($R_{l,q} = X_{l,q}$) requires the following orthogonality condition to be fulfilled:

$$\left\langle \widetilde{p}_i(t - sT), \widetilde{p}_l(t - qT) \right\rangle = \delta_{i,l}\, \delta_{s,q}, \tag{5.3}$$

where $\delta_{a,b}$ is the Kronecker delta function, defined as $\delta_{a,b} = 1$ when $a = b$ and $\delta_{a,b} = 0$ when $a \neq b$.

A multicarrier waveform that satisfies the orthogonality condition in (5.3) is called an orthogonal waveform; for example, the orthogonal frequency division multiplexing (OFDM) waveform. Let us look at the prototype filters used for OFDM and see how they fulfill the orthogonality condition. For an ith subcarrier in OFDM, the prototype filter is given by

$$\widetilde{p}_i(t) := \widetilde{p}(t)\, \mathrm{e}^{j2\pi f_i t}\,, \tag{5.4}$$

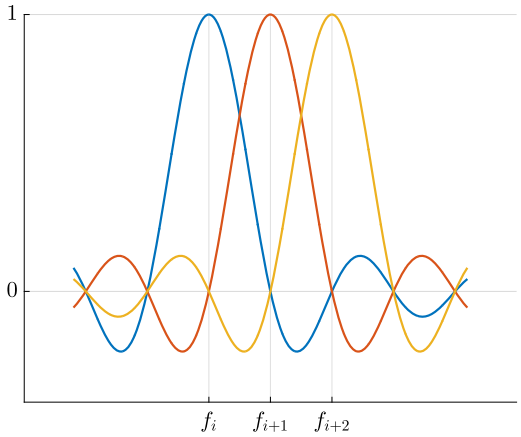

FIGURE 5.3

Frequency domain illustration of OFDM subcarriers.

where $f_i = \frac{i}{T}$ and $\widetilde{p}(t)$ is a rectangular filter with length T defined as

$$\widetilde{p}(t) := \begin{cases} \frac{1}{\sqrt{T}} & \text{if } 0 \le t \le T \\ 0 & \text{elsewhere} \end{cases}, \tag{5.5}$$

where the scaling $\frac{1}{\sqrt{T}}$ is simply chosen to get unit energy, i.e., $\int_{-\infty}^{+\infty} |\widetilde{p}(t)|^2 \, dt = 1$. Without loss of generality, the inner product (cf. (5.3)) between the prototype filters is given by

$$\begin{aligned} \langle \widetilde{p}_i(t), \widetilde{p}_l(t) \rangle &= \int_0^T \widetilde{p}_i(t) \, \overline{\widetilde{p}_l(t)} \, dt \\ &= \int_0^T \widetilde{p}(t) \, \mathrm{e}^{j2\pi f_i t} \, \widetilde{p}(t) \, \mathrm{e}^{-j2\pi f_l t} \, dt \\ &= \int_0^T \mathrm{e}^{j2\pi (f_i - f_l) t} \, dt \\ &= \int_0^T \mathrm{e}^{j2\pi \frac{i-l}{T} t} \, dt, \end{aligned}$$

which is nonzero (and equal to 1) if and only if $i = l$. We observe that it is the selection of $f_i = \frac{i}{T}$ that makes the OFDM waveform orthogonal. A frequency domain illustration of the OFDM subcarriers is shown in Fig. 5.3. The spacing between consecutive subcarriers is $f_{i+1} - f_i = \frac{i+1}{T} - \frac{i}{T} = \frac{1}{T} := \Delta f$, i.e., the subcarrier spacing Δf is the inverse of the symbol duration T.

When the orthogonality condition is not fulfilled, the waveform is nonorthogonal, for example, the FBMC waveforms. In the FBMC waveforms, the prototype filters of the subcarriers are not orthogonal within the same symbol as well as between the adjacent symbols. Typically, there is interference be-

tween subcarriers of the same symbols and between subcarriers of the adjacent different symbols (due to overlapping waveform symbols in the time domain). The inner product (based on (5.3)) takes the following form:

$$\left\langle \widetilde{p}_i(t-sT), \widetilde{p}_l(t-qT) \right\rangle = \begin{cases} 1 & \text{if } i=l \text{ and } s=q \\ \varepsilon_{i,l} & \text{if } i\neq l \text{ and } s=q, \\ \beta_{i,l,s,q} & \text{else,} \end{cases} \tag{5.6}$$

where $\varepsilon_{i,l}$ corresponds to an interference between subcarriers of the same symbol and $\beta_{i,l,s,q}$ is associated with an interference between subcarriers of two different symbols. These two types of interference are known as self-interferences—$\varepsilon_{i,l}$ is referred to as self-intercarrier interference and $\beta_{i,l,s,q}$ is referred to as self-intersymbol interference. The structure of the FBMC waveforms will be discussed in Section 5.1.3.

5.1.2 OFDM-BASED WAVEFORMS

There are several OFDM-based waveforms. In the following, we will present four major variants of the OFDM waveform, namely, CP-OFDM, windowed OFDM (W-OFDM), filtered OFDM (F-OFDM), and universally filtered OFDM (UF-OFDM).

A general discrete-time OFDM-based waveform is given by

$$x[n] = \left(\sum_{s\in\mathbb{Z}} \sum_{i\in I} X_{i,s}\ p_i[n-sN_{sc}] \right) * w_{tx}[n], \tag{5.7}$$

where I contains indices of the active subcarriers,[1] N_{sc} is the total number of subcarriers, $X_{i,s} \in \mathbb{C}$ is the modulated symbol corresponding to the subcarrier i and the time index s, $p_i[n] := p[n]\mathrm{e}^{j2\pi \frac{i}{N_{sc}} n}$ is the prototype filter (or pulse shape) used for the subcarrier i, and $w_{tx}[n]$ is a filter to improve spectral characteristics of the transmitted signal.[2] The modulation and demodulation operations of the OFDM-based waveforms are shown in Fig. 5.4 and Fig. 5.5, respectively.

5.1.2.1 Cyclic Prefix OFDM

CP-OFDM employs a rectangular pulse shape, i.e., $p[n]$ in (5.7) is given by

$$p[n] := \begin{cases} \frac{1}{\sqrt{N_{sc}}} & \text{if } 0 \le n \le N_{sc}-1, \\ 0 & \text{elsewhere,} \end{cases} \tag{5.8}$$

where N_{sc} is the total number of subcarriers. There is no post filtering operation, i.e., $w_{tx}[n] = \delta[n]$ in (5.7). To combat the intersymbol interference (ISI) in a multipath channel, a cyclic prefix (CP)

[1] In a multicarrier system, the number of active subcarriers is usually chosen smaller than the total number of subcarriers to relax filtering operations.

[2] The sharper the spectrum roll-off of the signal, the easier it is to fulfill the out-of-band (OOB) emission requirements specified by the 3GPP for cellular systems. The OOB emission requirements are specified in terms of a spectrum emission mask and an adjacent channel leakage ratio for both base stations and devices.

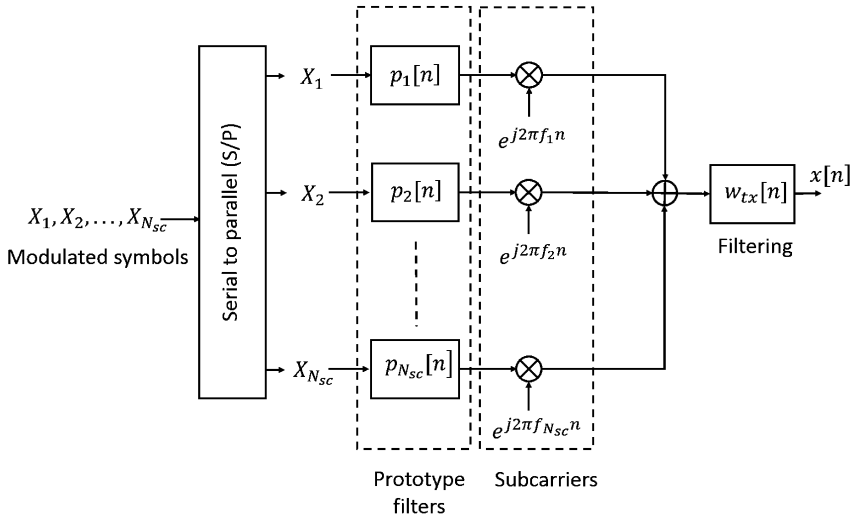

FIGURE 5.4

A general modulation structure of OFDM waveforms.

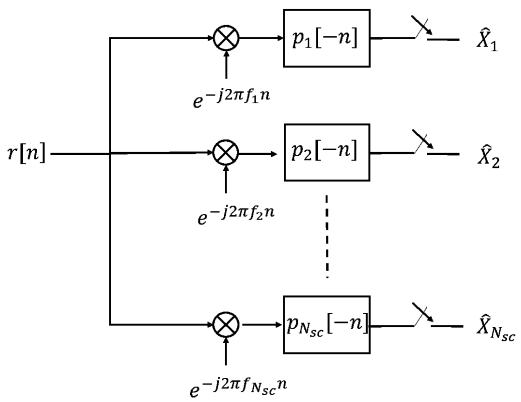

FIGURE 5.5

A general demodulation structure of OFDM waveforms.

is inserted in the OFDM symbol. The CP refers to the cyclic extension of an OFDM symbol, that is, appending the last N_{cp} samples of the OFDM symbol to the front of the symbol as illustrated in Fig. 5.6. If the CP duration is chosen greater than the delay spread of the channel, then the received OFDM signal does not suffer from any ISI. In LTE, the normal CP duration is 7% of the core OFDM symbol (i.e., $N_{sc} = 2048$ samples and $N_{cp} = 144$ samples).

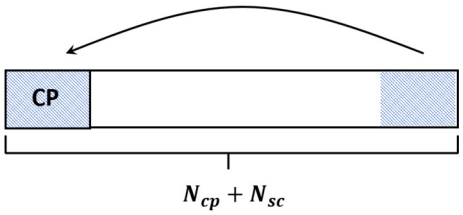

FIGURE 5.6

Cyclic prefix is inserted to avoid intersymbol interference due to the multipath channel.

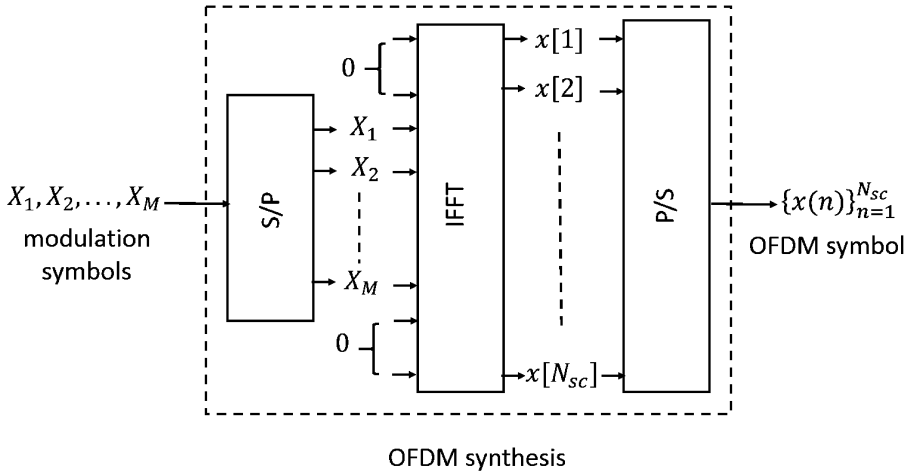

FIGURE 5.7

OFDM waveform is efficiently synthesized via fast Fourier transform.

In practice, CP-OFDM modulator is implemented via the computationally efficient fast Fourier transform (FFT). As shown in Fig. 5.7, M modulated QAM symbols ($\{X_i\}_{i=1}^{M}$) are mapped to orthogonal subcarriers via a serial-to-parallel (S/P) transformation followed by an IFFT of size N and parallel-to-serial (P/S) conversion. In this example, the total number of subcarriers is N and the number of active subcarriers is equal to M. In practice, the number of active subcarriers is kept smaller than the total number of subcarriers to relax filtering operations. This is achieved by zero padding QAM symbols prior to the IFFT operation, as shown in Fig. 5.7.

5.1.2.2 Windowed OFDM

The spectrum of CP-OFDM decays rather slowly. The main reason for its slow decay is the signal discontinuities at the symbol boundaries due to the rectangular pulse shape used in OFDM (cf. (5.8)). To improve the spectral shape of OFDM, a nonrectangular pulse shape $p[n]$ with smooth edges can be employed in (5.7), which we refer to as windowed-OFDM (W-OFDM) waveform. As an example,

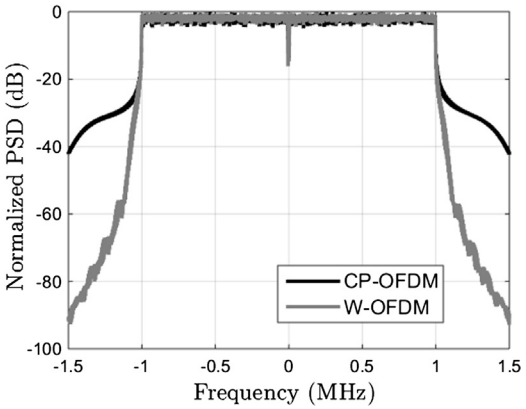

FIGURE 5.8

PSDs of CP-OFDM and W-OFDM waveforms.

the spectrum of W-OFDM (considering a window with linear slopes) is compared with CP-OFDM in Fig. 5.8. We observe that W-OFDM has a much sharper spectrum roll-off.[3]

The windowing can be done either at the transmitter side (to suppress interference to adjacent bands) or at the receiver side (to suppress interference pick-up from adjacent bands) [10,14]. In the following, we explain the transmitter side and the receiver side windowing. The transmitter side windowing is illustrated in Fig. 5.9. In the transmitter side windowing, the boundaries of each OFDM symbol are multiplied with a smooth slope in the time domain, increasing smoothly from 0 to 1 (increasing slope) or decreasing smoothly from 1 to 0 (decreasing slope). The increasing slope is applied at the beginning of the CP, while the decreasing slope is applied after the end of the core OFDM symbol within an extra added cyclic suffix. Fig. 5.9 also shows that the increasing slope of the next OFDM symbol overlaps with the decreasing slope of the previous OFDM symbol. Since the receiver only keeps the samples of the core OFDM symbol, the transmitter side windowing is transparent to the receiver. Next, we discuss the receiver side windowing.

A standard OFDM receiver cuts out the desired OFDM symbol period by applying a rectangular window in the time domain to the received signal and then subsequently applies the FFT for demodulating the subcarriers. Application of the rectangular window in the time domain corresponds to a convolution in the frequency domain with a sinc function. The sinc-like function leads to a high interference pick-up from any adjacent nonorthogonal signals such as OFDM signals with other numerologies. To reduce the interference pick-up, the rectangular window must be replaced by a smooth window function. The receiver side windowing operation is illustrated in Fig. 5.10. A smooth increasing window slope is applied at the boundary between the CP and the core OFDM symbol (half within each); a decreasing smooth window slope is applied at the boundary between the core OFDM symbol and the added cyclic suffix. If the applied window slopes fulfill the Nyquist criterion (i.e., they are

[3]The sharper the spectrum roll-off of the signal, the easier it is to fulfill the out-of-band emission requirements specified by the 3GPP for cellular systems.

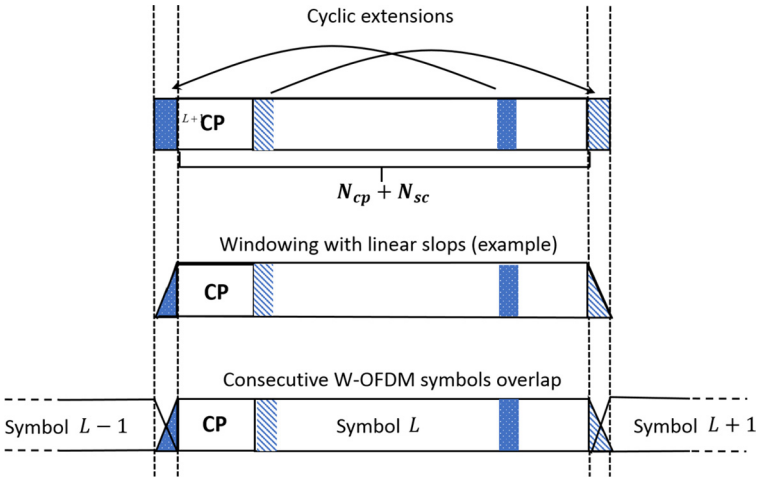

FIGURE 5.9

The transmitter side windowing.

center symmetric), the signal part cut away by the decreasing windowing slope is the same as the remaining signal part after application of the increasing window slope within the CP, since the CP is a copy of the last part of the OFDM symbol. If the windowed CP part is added to the last part of the core OFDM symbol, the core OFDM symbol is restored at its second boundary. The core OFDM symbol can also be restored at the first symbol boundary by applying the same trick. Now the complete OFDM is restored, and its subcarriers are orthogonal again. The FFT is applied to the restored core OFDM symbol as indicated in Fig. 5.10.

5.1.2.3 Filtered OFDM

Like windowing (or pulse shaping), filtering is another technique to improve spectral characteristics or reduce out-of-band (OOB) leakage of OFDM waveform [16]. Filtering (like windowing) is typically done at both transmitter and receiver sides to reduce interference to adjacent bands and reduce interference pick-up from adjacent bands, respectively. Let us refer to the general OFDM waveform modulation structure in (5.7). In filtered OFDM (F-OFDM), the prototype filter (pulse shape) $p[n]$ is rectangular including the CP, as we have in CP-OFDM. In addition, a filter $w_{tx}[n]$ is employed to suppress OOB leakage (cf. Fig. 5.4). The filter $w_{tx}[n]$ is derived as the product of an ideal bandpass filter impulse response and a time domain mask (or a window), that is,

$$w_{tx}[n] = h[n]w[n], \tag{5.9}$$

where $h[n]$ is an ideal bandpass filter with the selected signal bandwidth and $w[n]$ is a window function. Various window functions are common for the construction of FIR filters with different characteristics, for example, Hanning, Hamming, Blackman, Bartlett, and Kaiser window functions.

The filter $w_{tx}[n]$ is dependent on the signal bandwidth, which implies that the filter need to be dynamically designed or selected based on the signal bandwidth. This is different from W-OFDM,

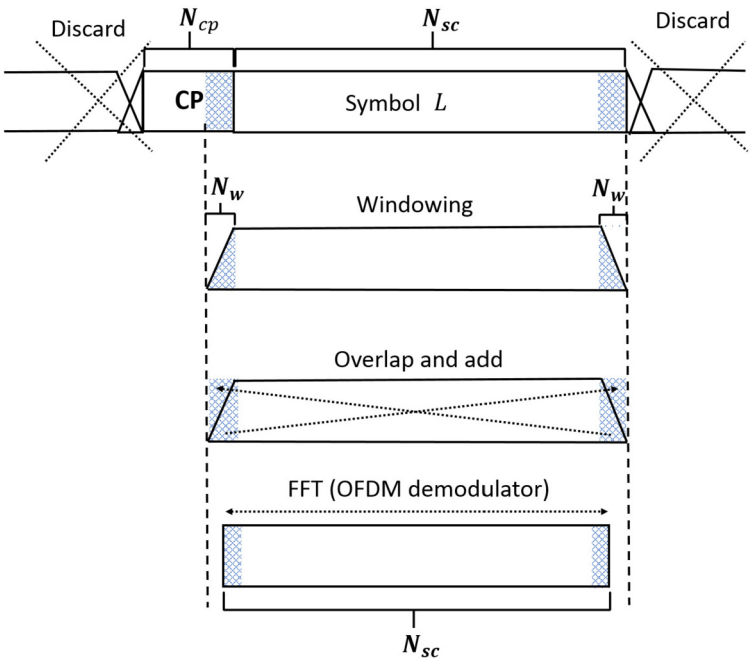

FIGURE 5.10

The receiver side windowing.

whose construction does not change with the signal bandwidth (i.e., the pulse shape $p[n]$ does not change with signal bandwidth). Another aspect of F-OFDM is that when long filters are used for an improved OOB suppression, there can be significant group delay due to the filtering. For example, if filters with length equal to half OFDM symbol are used at the transmitter and at the receiver sides, then the filter processing delay is equal to one OFDM symbol. The large processing delay increases overhead for TDD link direction switching, which is not suitable for latency critical applications.

5.1.2.4 Universally Filtered OFDM

UF-OFDM waveform is synthesized by performing filtering on groups of subcarriers (subbands) to improve the spectral shape (reduce OOB leakage) of each subcarrier group (subband) [12,9]. The subcarrier group-wise (subband) filtering is motivated by the fact that the scheduling operation in cellular systems (e.g., LTE and NR) is done based on subbands (resource blocks[4]). The subband filtering improves spectral characteristics. As an example, the spectrum of W-OFDM is compared with CP-OFDM in Fig. 5.11.

The transmitter structure of UF-OFDM is illustrated in Fig. 5.12. We assume that there are M active subcarriers and the subband filtering is performed on groups of B subcarriers (i.e., each subband

[4]In 4G LTE and 5G NR, a resource block comprises of 12 subcarriers.

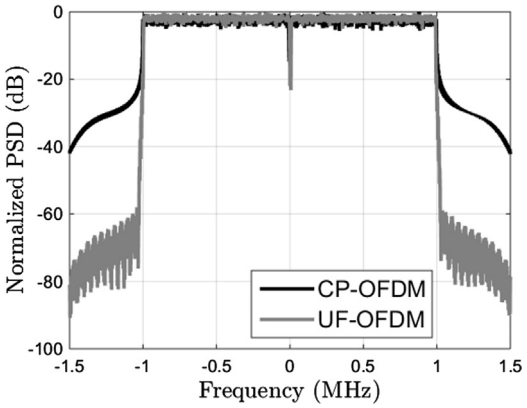

FIGURE 5.11

PSDs of CP-OFDM and UF-OFDM waveforms.

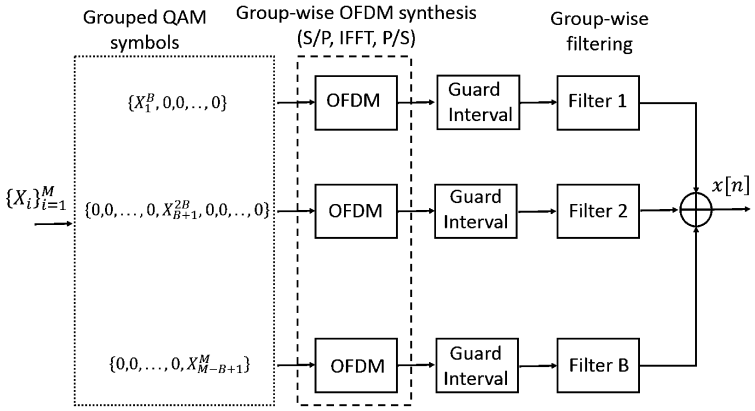

FIGURE 5.12

UF-OFDM transmitter structure.

has B subcarriers). As shown in Fig. 5.12, a set of QAM modulated symbols $\{X_1, X_2, \ldots, X_M\}$ are first divided into groups and zero padded. Each zero padded group follows the same process as we have for the OFDM synthesis, i.e., serial-to-parallel conversion, N_{sc}-point IFFT, and parallel-to-serial conversion. Afterwards, each symbol is padded with zeros in the time domain (i.e., a guard interval (GI) is inserted for each symbol) and filtered. The GI is inserted to prevent intersymbol interference due to the transmit filter delay. For an ISI free UF-OFDM synthesis, the GI length should be at-least equal to the filter length, as illustrated in Fig. 5.13.

The receiver processing of the UF-OFDM waveform is shown in Fig. 5.14. UF-OFDM waveform does not contain the CP, therefore, the cyclic convolution property is not preserved. Unlike the CP-OFDM demodulator that discards the CP part of the symbol before the FFT operation, the UF-OFDM

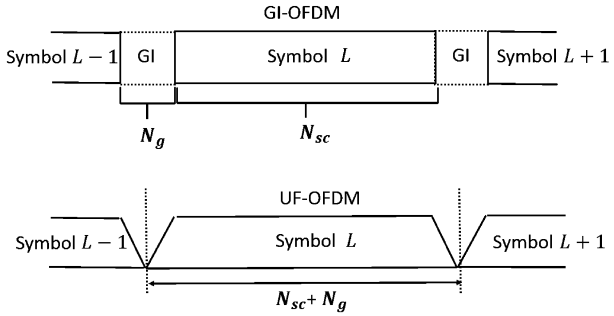

FIGURE 5.13

A guard interval is required for interference-free filtering in UF-OFDM modulator.

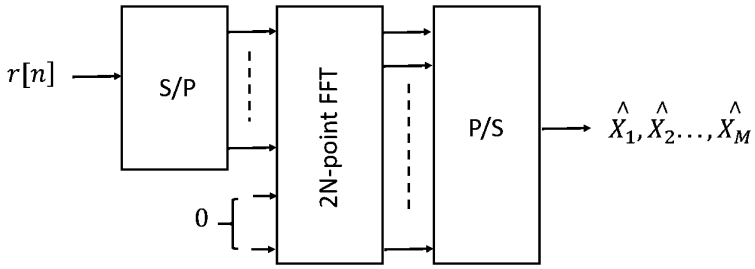

FIGURE 5.14

UF-OFDM receiver structure.

receiver utilizes complete symbol including the GI part in the demodulation. A $2N_{sc}$ point fast Fourier transform (FFT) is performed to recover the data. From the FFT output block (of size $2N_{sc}$), only the even indexed symbols are the desired reconstructed QAM symbols. For details, we refer the reader to [12,11].

5.1.3 FILTER BANK-BASED WAVEFORMS

There is an inverse relation between time and frequency. That is, extending a signal in the time domain makes it shrink in the frequency domain. Based on this principle, the filter bank multicarrier (FBMC) waveforms employ pulse shapes (prototype filters) with a much longer time duration than the OFDM-based waveforms to achieve a more confined spectrum. Spectral confinement is important for efficient utilization of the spectrum, which is a precious resource. However, as the waveform symbols get longer in the time domain, the adjacent waveform symbols overlap. (Non-overlapping symbols would result in loss of data transmission rate.) The FBMC waveforms are not orthogonal. That is, even in the absence of any channel impairment, it is not possible to perfectly reconstruct the QAM symbols transmitted using an FBMC waveform.

A conceptual illustration of the FBMC transmitter is given in Fig. 5.15. We note that conceptually the construction of FBMC is similar to OFDM-based waveforms (e.g., W-OFDM), however, with the

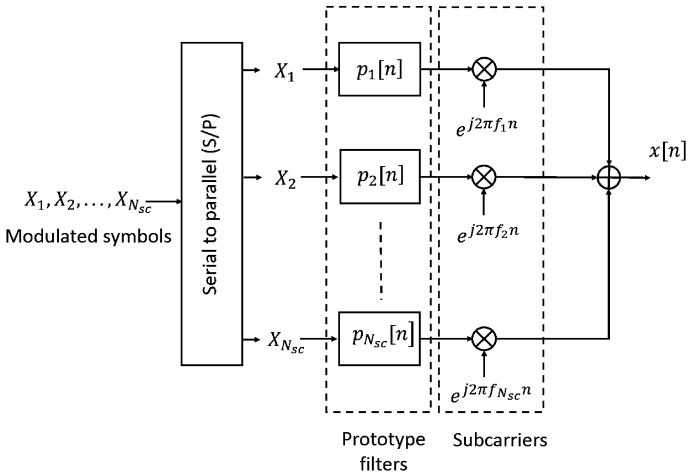

FIGURE 5.15

A conceptual illustration of FBMC modulator.

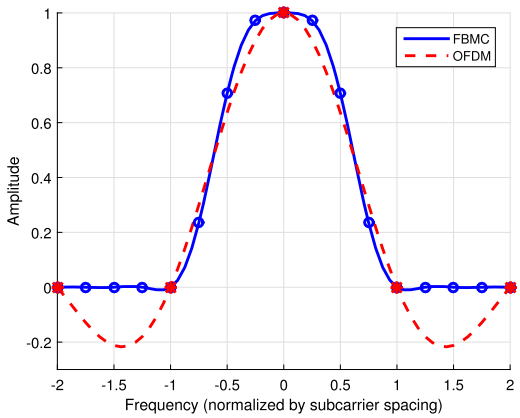

FIGURE 5.16

Frequency responses of the prototype filters of OFDM and FBMC ($K = 4$). The respective frequency domain coefficients are given in Table 5.1.

important difference that the length of the prototype filter is approximately K times greater than the prototype filter (window/pulse) used in the OFDM-based waveforms. For FBMC, the duration of the prototype filter $p_i[n]$ is KN_{sc} samples. The prototype filters for FBMC can be synthesized via frequency domain oversampling of the (rectangular) prototype filter used for OFDM. That is, a prototype filter of length KN_{sc} can be constructed by oversampling the frequency response with a factor K. In Fig. 5.16, we show an example of an oversampled frequency response of the rectangular prototype

Table 5.1 Frequency domain coefficients of the FBMC prototype filters

Waveform	H[0]	H[1]	H[2]	H[3]
OFDM	1	0	0	0
FBMC ($K=2$)	1	$\sqrt{(2)}/2$	0	0
FBMC ($K=3$)	1	0.911438	0.411438	0
FBMC ($K=4$)	1	0.971960	$\sqrt{(2)}/2$	0.235147

The filters have symmetric frequency response, i.e., H[k]=H[-k]

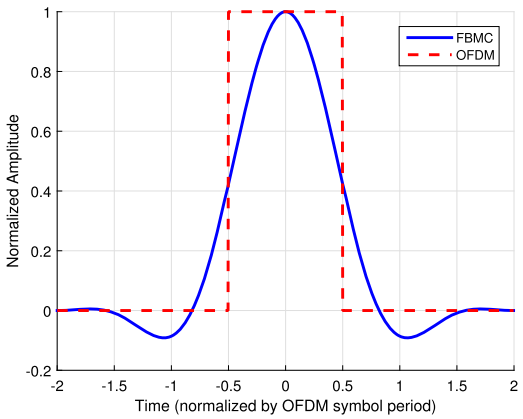

FIGURE 5.17

Impulse responses of the prototype filters used in FBMC ($K=4$) and OFDM.

filter (used in OFDM) with a factor $K=4$. The frequency axis in Fig. 5.16 is normalized by $\frac{1}{N_{sc}}$ which is the subcarrier spacing in OFDM and FBMC waveforms. The frequency domain coefficients of the filters are given in Table 5.1. The corresponding time domain representations of these filters are given in Fig. 5.17. The time axis here is normalized by the number of samples in the OFDM symbol without the CP (N_{sc}). The prototype filter is designed to be half-Nyquist, that is, convolution of the transmitter side half-Nyquist and the receiver side half-Nyquist filter is a Nyquist filter that crosses zero (on the time axis) at all the integer multiples of the symbol period [2].

The design, implementation, and characteristics of the prototype filters are discussed in great detail in [2,1]. There are two commonly used methods for implementing FBMC: frequency spreading (FS) and polyphase networks (PPN). In the frequency spreading (FS) method, offset QAM (OQAM) symbols are filtered in the frequency domain, followed by a KN_{sc} point IFFT and an overlap and sum operation. At the receiver side, a sliding window selects KN_{sc} points every $N_{sc}/2$ samples. A KN_{sc} point FFT is performed followed by a matched filtering. In the PPN based FBMC transmitter, an N_{sc} point IFFT is performed on OQAM symbols. The IFFT output (time domain signal) is fed to a polyphase network. At the receiver side, matched filtering is performed followed by a N_{sc} point FFT [2].

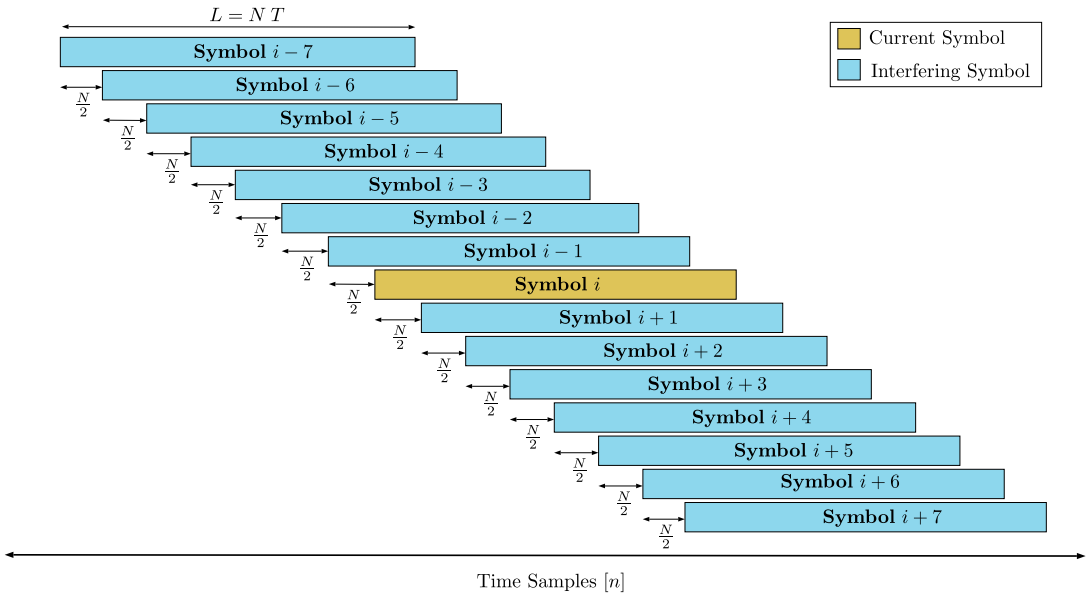

FIGURE 5.18

The overlapping symbol structure of FBMC-OQAM with overlapping factor $K = 4$.

As mentioned earlier, the FBMC waveforms are not orthogonal. There are two reasons for the non-orthogonality:

1. **Intersymbol Interference** An FBMC symbol spans $K N_{sc}$ samples, therefore, the neighboring FBMC symbols overlap as shown in Fig. 5.18. There is a time offset N_{sc} between the adjacent symbols. Due to the overlapping symbols, there is intersymbol interference (ISI) [2]. For a given subcarrier of an FMBC symbol, the ISI primarily comes from the direct adjacent subcarriers of the other overlapping FBMC symbols, i.e., a kth subcarrier in an FBMC symbol primarily suffers interference from subcarriers k and $k-1$ of the overlapping FBMC symbols. The ISI from the subcarriers that are further than the direct neighboring subcarriers is negligible (uniformly upper bounded by -60 dB [2]). There is no ISI between same subcarriers of the overlapping FBMC symbols due to the Nyquist property of the prototype filters [2].
2. **Intercarrier Interference** The subcarriers within an FBMC symbol are not orthogonal either [2]. We refer to this as intercarrier interference (ICI). The ICI primarily comes from the adjacent subcarriers (as in the case of the ISI). For any adjacent subcarriers, there is interference between the real parts or the imaginary parts, but there is no interference between the real and the imaginary parts. To eliminate the ICI between the real parts (or the imaginary parts) of the adjacent subcarriers, they have to be offset by $N_{sc}/2$ samples. This property motivates employing the OQAM modulation, where the subcarriers of the FBMC symbol are modulated with an alternating pattern of real and imaginary valued symbols [2].

Broadly speaking, the FBMC waveforms can be divided into two types—one that employs the offset QAM and one that employs the regular QAM. In the following, we briefly discuss both types.

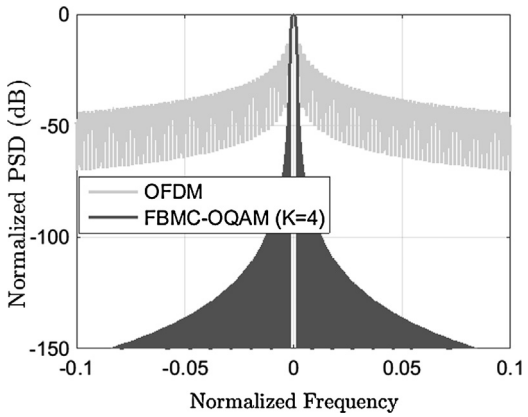

FIGURE 5.19

Comparison of spectrum of OFDM and FBMC-OQAM for one subcarrier.

5.1.3.1 FBMC-OQAM

A discrete-time FBMC-OQAM signal is given by

$$x[n] = \sum_{s\in\mathbb{Z}} \sum_{i\in I} X_{i,s}\, \theta_{i,s}\, p_i \left[n - s\frac{N_{sc}}{2} \right], \tag{5.10}$$

where the set I contains indices of the active subcarriers, N_{sc} is the total number of subcarriers, $X_{i,s} \in \mathbb{R}$ is the modulation symbol of the subcarrier i and the (FBMC) symbol time index s, $\theta_{i,s} := j^{i+s}$ is the phase rotation associated with the offset QAM mapping, $p_i[n] := p[n]\, \mathrm{e}^{j2\pi \frac{i}{N_{sc}} n}$ is the filter for the subcarrier i with $p[n]$ as the base filter with length $L = K\, N_{sc}$ (where K is the overlapping/oversampling factor). The overlapping factor K is a parameter of the FBMC-QAM waveform which refers to the property that a given FBMC-OQAM symbol overlaps with $2K - 1$ symbols preceding it and $2K - 1$ symbols following it. Furthermore, $D = \{-2K + 1, ..., 2K - 1\}$ denotes the set of the adjacent FBMC symbols that overlap in time. An illustration of the overlapping symbol structure is given in Fig. 5.18 with a symbol overlapping (or frequency domain oversampling) factor $K = 4$.

Next, we compare spectral shapes of OFDM and FBMC-OQAM waveforms considering the widely adopted FBMC prototype filters [2,1]. The frequency domain coefficients $H[k]$ of these prototype filters are given in Table 5.1 for three different oversampling (overlapping) factors. The frequency response is symmetric around the center frequency (which is necessary for ensuring the Nyquist property), i.e., $H[-k] = H[k]$. (The prototype filter in Fig. 5.16 and Fig. 5.17 is also constructed using the coefficients given in Table 5.1.) In Figs. 5.19–5.22, we compare power spectral densities of OFDM and FBMC-OQAM waveforms with different overlapping (oversampling) factors. The comparisons include the spectrum of a single subcarrier as well as of a group of 300 subcarriers. These results show that FBMC-OQAM has significantly sharper spectral roll-off than OFDM, especially for $K \geq 3$. The overlapping factor $K = 4$ is most commonly used in the literature.

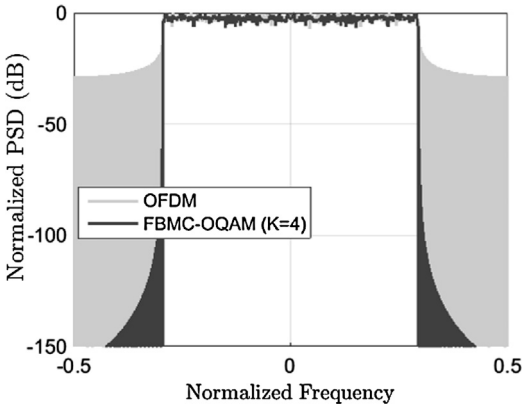

FIGURE 5.20

Comparison of spectrum of OFDM and FBMC-OQAM for 300 subcarriers.

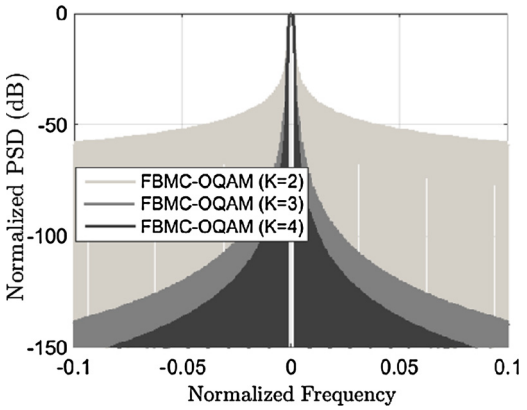

FIGURE 5.21

Comparison of spectrum of one subcarrier of FBMC-OQAM for different overlapping factors.

5.1.3.2 FBMC-QAM

An FBMC waveform that employs a regular QAM (instead of the offset QAM) is referred to as FBMC-QAM. As discussed earlier, there can be significant interference between the real parts (or between the imaginary parts) of the adjacent subcarriers in an FBMC symbol. The offset QAM is one way to reduce the effect of interference from the adjacent subcarriers. Another approach is to design the prototype filters such that the self-interference is minimized or kept to an acceptable level so that the regular QAM can be employed. Typically, the self-interference can be reduced at the cost of degradation in spectral confinement. We will see this shortly in the sequel.

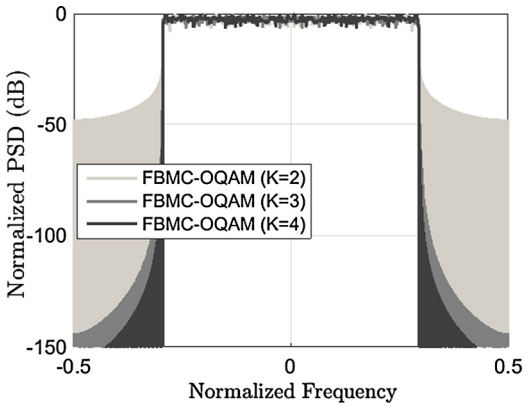

FIGURE 5.22

Comparison of spectrum of 300 subcarriers of FBMC-OQAM for different overlapping factors.

A discrete-time FBMC-QAM signal is expressed as

$$x[n] = \sum_{s\in\mathbb{Z}} \sum_{i\in I} X_{i,s}\; p_i[n - sN_{sc}]\,, \tag{5.11}$$

where I is the set of indices of the active subcarriers, N is the total number of subcarriers, $X_{i,s} \in \mathbb{C}$ is the modulated symbol corresponding to subcarrier i and time index s, and $p_i[n]$ is the filter for subcarrier i. The length of $p_i[n]$ is $L = K\,N$ and K is the overlapping factor. The overlapping factor K is a parameter of FBMC-QAM waveform which refers to the property that a given FBMC symbol overlaps with $K-1$ symbols preceding it and $K-1$ symbols following it. Thus, $D = \{-K+1, ..., K-1\}$ is the set containing indices of the adjacent FBMC symbols that overlap in time considering an overlapping factor K. An example is shown in Fig. 5.23 for a symbol overlapping (or the frequency domain oversampling) factor $K = 4$.

In the recent publications [8,13], a method to design multiple prototype filters (different filters for different subcarriers) has been developed for the synthesis of an FBMC-QAM waveform. To design the prototype filters, a constrained optimization problem is formulated with the objective function being self-interference and the constraints being the spectrum confinement described by falloff rate and the number of nonzero filter taps in the frequency domain. The prototype filters obtained through this method trade-off signal-to-interference ratio caused by the self-interference with spectrum confinement. In [8,13], the authors provide a design example with two prototype filters—one filter is used for the even-numbered subcarrier indices and the other filter is used for the odd-numbered subcarrier indices. That is,

$$p_i[n] := \begin{cases} p_{even}[n]\, \mathrm{e}^{j2\pi \frac{i}{N_{sc}} n} & \text{if } i \text{ is even,} \\ p_{odd}[n]\, \mathrm{e}^{j2\pi \frac{i}{N_{sc}} n} & \text{if } i \text{ is odd.} \end{cases} \tag{5.12}$$

The length of $p_{even}[n]$ and $p_{odd}[n]$ is $L = K\,N_{sc}$. Considering these two prototype filters (see [8,13] for the filter coefficients $p_{even}[n]$ and $p_{odd}[n]$) for FBMC-QAM, we compare its power spectrum

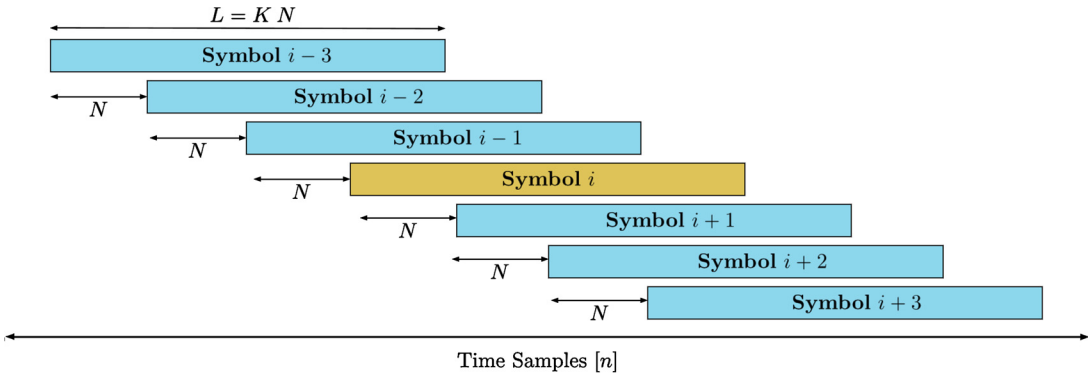

FIGURE 5.23

Overlapping symbol structure of FBMC-QAM with overlapping factor $K = 4$.

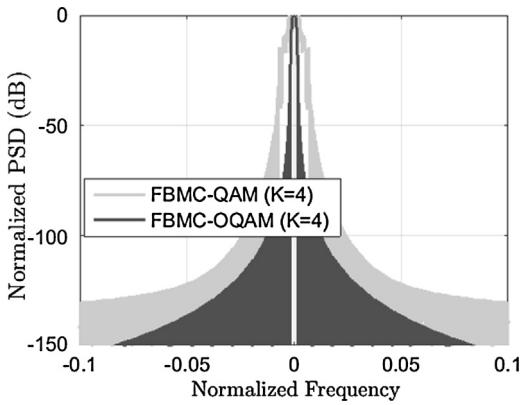

FIGURE 5.24

Comparison of spectrum of FBMC-QAM and FBMC-OQAM for one subcarrier.

with an FBMC-OQAM waveform for a single subcarrier as well for a group of 300 subcarriers in Fig. 5.24 and Fig. 5.25. We observe that the FBMC-OQAM has better spectral characteristics than the FBMC-QAM. A major benefit of FBMC-QAM is that it is better compatible with MIMO transmission due to the utilization of the complex valued QAM symbols.

An important attribute of the FBMC waveforms is that they typically do not employ any CP or GI, unlike the OFDM-based waveforms. The prototype filters in the FBMC waveforms have long decaying tails which can make them robust to the ISI caused by frequency-selective channels. By avoiding the CP overhead, the FBMC waveforms can potentially utilize transmission resources more efficiently than the OFDM-based waveforms, at least in theory. In order to compare the resource usage efficiency, we have sketched the time-frequency lattices for OFDM, FBMC-OQAM, and FBMC-QAM in Fig. 5.26, Fig. 5.27, and Fig. 5.28, respectively. In these figures, Δf denotes the subcarrier spacing

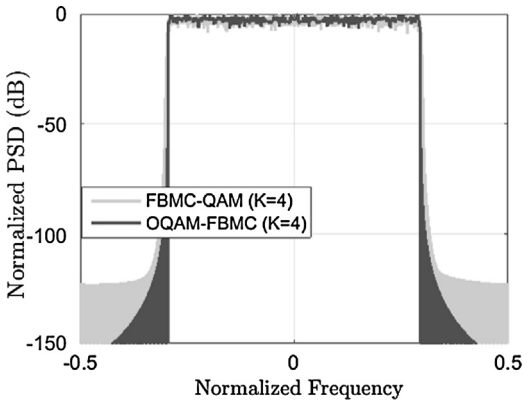

FIGURE 5.25

Comparison of spectrum of FBMC-QAM and FBMC-OQAM for 300 subcarriers.

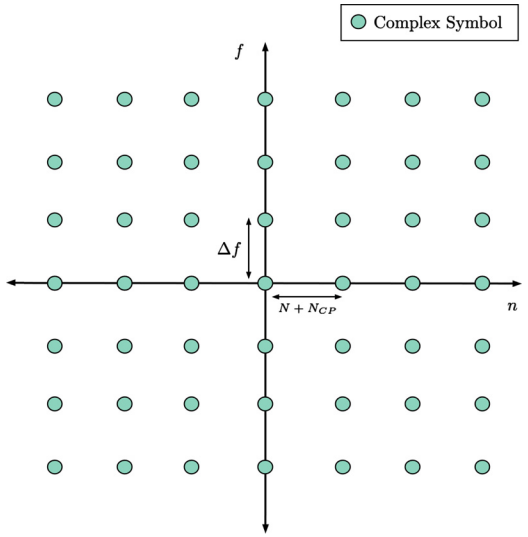

FIGURE 5.26

Time-frequency lattice representation for CP-OFDM.

(which is equal to $\frac{1}{N}$ for all waveforms), N denotes the total number of subcarriers (assumed equal for all waveforms), and N_{CP} is the number of CP samples in CP-OFDM. We observe that FBMC-QAM has one complex symbol per unit area on its lattice and FBMC-OQAM has two real symbols per unit area on its lattice. This means that the two FBMC waveforms have an equal resource usage efficiency. CP-OFDM has $\frac{N}{N+N_{CP}}$ (less than one) complex symbol per unit area, implying a lower resource usage efficiency than the FBMC waveforms. Although FBMC has better time-frequency re-

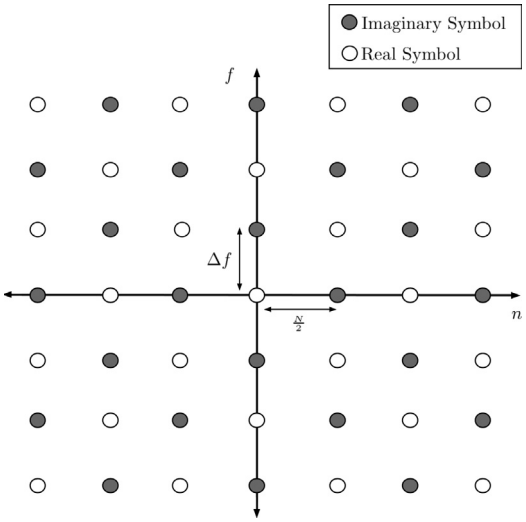

FIGURE 5.27

Time-frequency lattice representation for FBMC-OQAM.

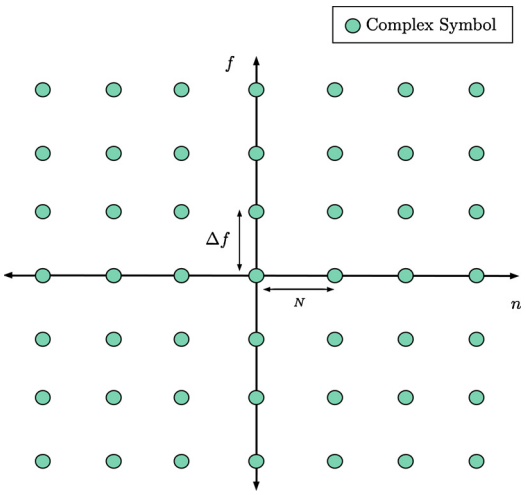

FIGURE 5.28

Time-frequency lattice representation for FBMC-QAM.

source utilization in theory, one cannot simply conclude that CP-OFDM has worse spectral efficiency in a realistic scenario. Here, it is important to keep in mind that the FBMC waveforms suffer from self-interferences (being nonorthogonal waveforms). Moreover, when the channel delay spread is large, the

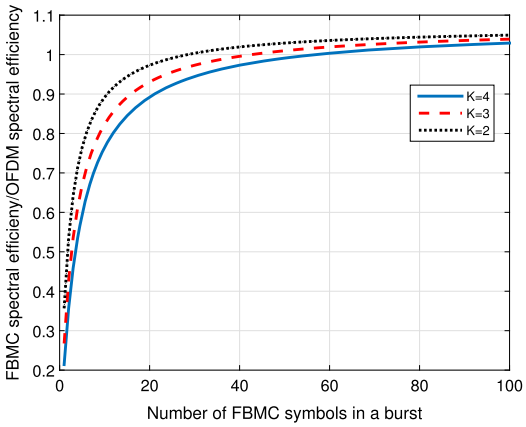

FIGURE 5.29

The ratio of FBMC and OFDM resource usage efficiencies as a function of the number of the waveform symbols per transmission burst.

FBMC waveforms can also have noticeable ISI due to the multipath effect and may require the CP overhead.

Another important aspect is that the time-resource usage efficiency of the FBMC waveforms depends on the transmission burst duration, whereas the time-resource usage efficiency of the OFDM waveforms does not depend on the burst duration. For example, if there are M FBMC symbols in a transmission burst (time slot), then the burst duration has to be $(M + K - 1)N_{sc}$ samples due to the fact that each FBMC symbol has length KN_{sc} and the consecutive FBMC symbols overlap with an offset N_{sc}. This implies that the time-resource usage efficiency of FBMC is $\frac{M}{M+K-1}$. For the OFDM waveform the time-resource utilization efficiency is $\frac{N}{N+N_{CP}}$, regardless of the transmission burst duration. In Fig. 5.29, we plot the ratio of the resource utilization efficiencies of the FBMC and OFDM waveforms. We observe that OFDM is more efficient for shorter transmission burst durations, which is especially important for delay sensitive applications. For LTE, a subframe consists of merely 14 OFDM symbols and therefore OFDM is suitable for LTE like assumptions. In NR, a transmission burst can be as short as one OFDM symbol to support latency critical applications (see Section 2.3 for the mini-slot based transmission).

5.2 SINGLE CARRIER DFTS-OFDM

Multicarrier waveforms, including OFDM, have large variations in instantaneous amplitude (and power) due to the superposition of a large number of modulated subcarriers. When there are large variations in the amplitude of the transmit signal, the power amplifiers of the transmitter either operate in a nonlinear region and cause signal distortion (due to nonlinear clipping) or the transmitter dissipates more power in order to operate in a linear region and prevent distortions. In contrast, single-carrier waveforms have small signal variations and therefore higher power efficiency than multicarrier

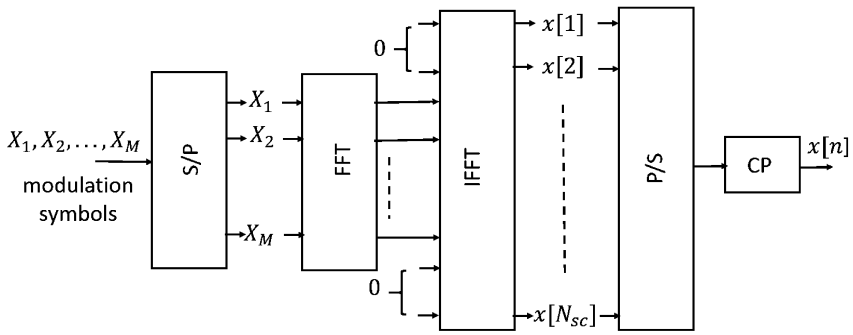

FIGURE 5.30

DFTS-OFDM transmitter structure.

waveforms. For example, there exist constant envelope single-carrier waveforms (e.g., minimum shift keying (MSK), Gaussian minimum shift keying (GMSK)) that allow power amplifiers to run at saturation point without any need for precompensation or postcompensation to account for the clipping. The single carrier PSK modulated waveform also has a constant amplitude. However, pure single-carrier waveforms have their disadvantages—a low spectral efficiency, performance degradation in frequency-selective channels, and lack of flexible resource allocation in the frequency domain. The single-carrier DFT spread OFDM (DFTS-OFDM) waveform aims at combining benefits of the single-carrier and the multicarrier waveforms, with the following key properties:

- Small amplitude variations (single-carrier aspect).
- Flexible resource allocation in the frequency domain (multicarrier aspect).

DFTS-OFDM can be seen as an OFDM waveform with DFT-based precoding (which makes it single-carrier) [7]. The structure of the DFTS-OFDM modulator is shown in Fig. 5.30. An M-point FFT (DFT) is performed on M QAM symbols followed by an N_{sc}-point IFFT with $M < N_{sc}$. A cyclic prefix is inserted as in CP-OFDM to enable low complexity frequency domain equalization at the receiver side. Fig. 5.31 compares the peak-to-average power ratios of CP-OFDM and DFTS-OFDM waveforms via the complementary cumulative distribution function (CCDF) of PAPR, assuming 16 QAM modulation and 1200 subcarriers. CCDF shows the likelihood of PAPR (in terms of percentage) exceeding a given value. We observe a reduced PAPR with DFTS-OFDM. If one employs PSK modulation instead of QAM, PAPR of DFTS-OFDM can be further reduced.

The bandwidth of a DFTS-OFDM signal is given by $\frac{M}{N} f_s$, where f_s is the sampling frequency. The instantaneous signal bandwidth can vary by changing the block size M, to allow for flexible bandwidth assignment. Moreover, users can be multiplexed in the frequency domain by allocating subsets of subcarriers to different users. For example, according to Fig. 5.30, if we want to multiplex two users with equal bandwidths, the first $\frac{M}{2}$ QAM symbols $(X_1, X_2, \ldots, X_{M/2})$ can be associated with user 1 and the last $\frac{M}{2}$ QAM symbols $(X_{M/2}, X_{M/2+1}, \ldots, X_M)$ can be associated with user 2 (assuming M is even). In this example, each user is assigned contiguous subcarriers. Alternatively, each user can also be assigned noncontiguous subcarriers. For example, user 1 and user 2 can be interleaved by assigning odd-numbered subcarriers (i.e., modulation symbols $X_1, X_3, \ldots, X_{M-1}$) to user 1 and even-numbered

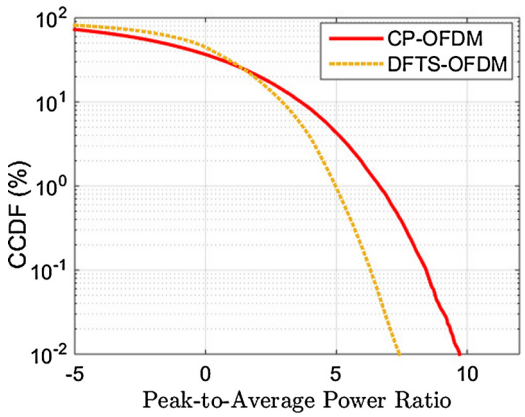

FIGURE 5.31

DFTS-OFDM achieves much reduced PAPR than CP-OFDM.

subcarriers (i.e., modulation symbols $X_2, X_4, \ldots, X_M$) to user 2. When multiple users are multiplexed in DFTS-OFDM waveform, it is often referred to as single-carrier frequency division multiple access (SC-FDMA). If users are assigned contiguous subcarriers, it is called localized frequency division multiple access (LFDMA). When each user is assigned noncontiguous subcarriers that are uniformly distributed across its bandwidth, it is commonly known as interleaved frequency division multiple access (IFDMA).

DFTS-OFDM is used in 4G LTE for the uplink transmissions due to its improved power efficiency. It is also an optional waveform for the 5G NR uplink. However, there are some shortcomings of employing DFTS-OFDM, which are discussed in Chapter 6.

5.3 WAVEFORM DESIGN REQUIREMENTS FOR 5G NR

5G radio access will support various applications (eMBB, URLLC, massive machine type communications (mMTC)), a wide range of frequencies (from sub-1 GHz to 100 GHz), diverse deployments, and various link types (uplink, downlink, device-to-device link, backhaul link). In the following, we provide an overview of important waveform design requirements for different scenarios.

eMBB has high requirements on throughput, user density, and low latency. Both small and large cell deployments are expected for eMBB services. Typically, larger cells in low carrier frequencies in the licensed spectrum and small cells at higher carrier frequencies (e.g., millimeter-wave) in both the licensed and the unlicensed spectrum. For the downlink transmission, a high spectral efficiency and maximum utilization of MIMO are key requirements for the NR waveform. For the uplink transmissions in the large cell deployments, the cell edge users can be power limited and may not be able to achieve high spectral efficiencies. In this case, the power efficiency of the waveform is important. In the small cell deployments, the distance between the users and the base station can significantly reduce

but not necessarily the maximum transmission power of the users. In this case, the power efficiency and the MIMO compatibility are important design requirements.

At very high carrier frequencies (e.g., millimeter-wave), analog or hybrid beam-forming is expected, at least in the early stage of the NR deployments (see Chapter 7 for details). In such systems, the number of digital chains is small compared to the number of antennas and part of the beam-forming is realized via the RF beam-forming. With the RF beam-forming, it is not possible to multiplex users in the frequency domain (frequency division multiplexing (FDM)) unless they all are served by the same beam. In this case, the users should be multiplexed in the time domain (time division multiplexing (TDM)) and therefore a short transmit time interval (TTI) is important. The NR waveform has to be confined in time to allow for the short transmissions.

For the URLLC services, the ultra-reliability and very low latency are important. Beam-forming is an important tool for improving the reliability. To achieve a very low latency, the waveform should be confined in the time domain with a low processing latency. For a fast uplink access, an asynchronous transmission may be beneficial, which means that the waveform should be able to efficiently support the asynchronous access. The retransmission mechanisms are important for enhancing the link reliability. In order to reduce latency due to the HARQ, the waveform should efficiently support the short TTIs.

The mMTC use cases target at providing connectivity to a massive number of devices with strict requirements on battery life and processing complexity. mMTC applications are expected in large cell deployments at lower carrier frequencies (e.g., below 6 GHz). mMTC data traffic can be in the form of short data bursts. Moreover, the radio propagation and penetration losses can be high, for example, to provide connectivity to devices in the basement of a building. Hence, the important waveform design requirements for the mMTC are the high power efficiency (in the uplink), the low complexity transceiver processing, the suitability to the short burst durations, and the ability to multiplex large number of users. Asynchronous access can also be important in the uplink.

The D2D communication typically has short range; therefore, the power efficiency is not very important. For the D2D communication, requirements are expected to be high on throughput and therefore the spectral efficiency is important. Since the D2D links are symmetric in nature, it is desirable to have the same waveforms in both directions.

For the backhaul links (base station-to-base station communication), high throughputs and low latencies are important. The wireless backhaul or the self-backhaul is likely with small cell deployments. Hence, the most important waveform design requirements are high spectral efficiency, compatibility with MIMO, and low latency (similar to eMBB). In wireless backhauling, the links are symmetric in nature and, hence, the same waveform is desirable in both directions.

5.4 KEY PERFORMANCE INDICATOR FOR NR WAVEFORM DESIGN

Key characteristics of 5G NR include large channel bandwidths, extreme data rates, ultra-reliability and low latency requirements, harsh propagation conditions, severe RF impairments, massive number of antennas, small sized base stations, and mainly TDD deployments. Considering these aspects, the mmMAGIC project (a European research project[5]) as well as the 3GPP identified key performance

[5] mmMAGIC was an EU project (funded by H2020 program) that developed radio interface concepts and solutions for above 6 GHz mobile radio communications.

indicators (KPIs) for the NR waveform design and evaluated the candidate waveforms for these KPIs. In the following, we present these waveform design KPIs and their importance in different frequency ranges. The key performance indicators for the NR waveform design include:

- **Spectral efficiency** The spectral efficiency is vital to support extreme requirements on data rate, user connection, and traffic densities. In general, the spectral efficiency is more crucial at lower carrier frequencies than at higher frequencies, since the spectrum is not as precious at higher frequencies due to the availability of potentially much larger channel bandwidths.
- **MIMO compatibility** Multiantenna transmission is a driving technology for NR. With the increase in carrier frequency, the number of antenna elements would increase in the base stations as well as in the devices. The use of various MIMO schemes is essential in providing high spectral efficiencies (by enabling SU-MIMO/MU-MIMO) and greater coverage (via beam-forming). Beam-forming is instrumental in overcoming the high transmission losses at very high frequencies (coverage limited scenarios).
- **Low Peak-to-Average-Power-Ratio (PAPR)** A low PAPR is essential for power efficient transmissions from the devices (for example, uplink, sidelink). A low PAPR becomes even more important at very high frequencies. Since small sized low-cost base stations are envisioned at high frequencies, low PAPR is also important for the downlink transmissions.
- **Robustness to channel time selectivity** The robustness to channel time variations is vital in high vehicular speed scenarios. The high speed scenarios are relevant in large cell deployments. The large cell deployments are not expected at very high frequencies due to harsh propagation conditions (coverage limitation). At very high frequencies, the deployments are expected to come in the form of small cells where mobility is not a major concern. However, certain vehicular services may be enabled at very high frequencies.
- **Robustness to channel frequency selectivity** Typically, wideband wireless channels are strongly frequency selective and robustness to frequency selectivity is fundamental to support high throughput communication over wideband channels.
- **Robustness to phase-noise** Phase-noise depends on quality of the local oscillators at the devices and at the base stations. Typically, phase-noise is high due to the UE (transmitter/receiver), since low phase-noise oscillators can be too expensive and power consuming for the devices. Phase-noise robustness is also important for future low-cost base stations. Basically, any link that involves a device and/or low-cost base station puts a high requirement on the phase-noise robustness of the waveform; especially if the communication takes place at high frequencies since phase-noise typically increases with the carrier frequency (see Chapter 4).
- **Robustness to Power Amplifier Non-linearity** The impact of the nonlinear PA increases as the signal bandwidth increases (see Chapter 4).
- **Transceiver baseband complexity**, involved in encoding and decoding of the information embedded in a waveform. The baseband complexity is always very important for the devices, especially from the receiver perspective. For NR, the complexity is even a major consideration for base stations, since a base station can be a small sized access node (especially at high frequencies) with limited processing capability. At very high frequencies and large bandwidths, the receiver may also have to cope with severe RF impairments. A low baseband complexity is also important for faster processing and enabling low latency applications. Moreover, the baseband complexity becomes increasingly important as the signal bandwidth increases.

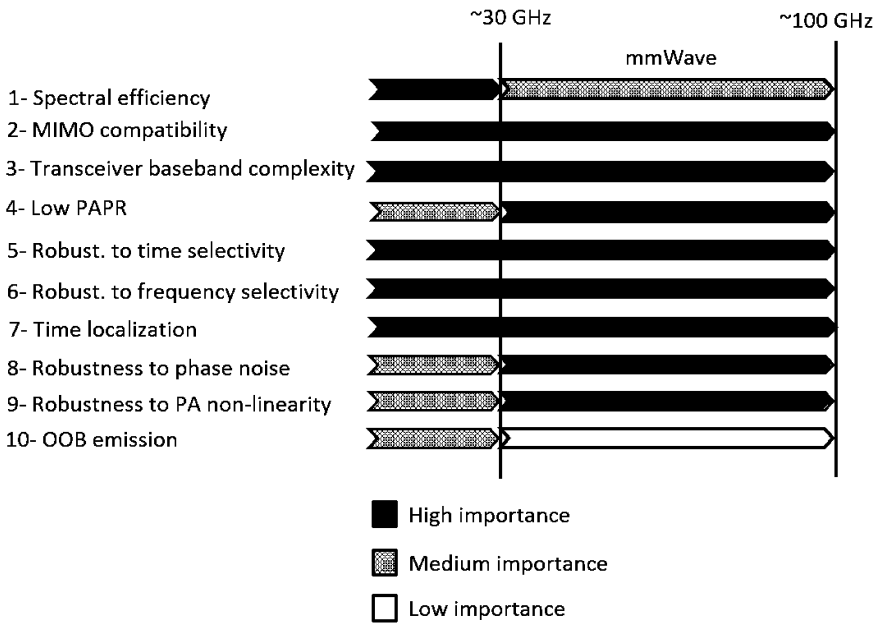

FIGURE 5.32

Importance of waveform performance indicators as a function of carrier frequency.

- **Time localization** Time localization is important to efficiently enable (dynamic) TDD and support low applications. Frequent link direction switching for TDD requires short burst transmissions. A low latency, which is one of the key requirements for both the eMBB and the URLLC services, also requires short transmission time slots. A waveform that is confined in the time domain is suitable for enabling short transmissions.
- **Out-of-band emissions/Frequency localization**: Frequency localization is useful for efficient utilization of spectrum and potential multiplexing of different services (e.g., URLLC, mMTC, eMBB) on a single carrier using different waveform numerologies (see Section 6.3.3). Frequency localization is not a major performance indicator at high frequencies where large channel bandwidths are available. Frequency localization is also relevant for asynchronous access, which can be useful in uplink and sidelink.
- **Flexibility and scalability** Flexibility and scalability of the waveform is important to enable diverse use cases and deployment scenarios.

Fig. 5.32 sketches importance of the waveform KPIs for the NR operation in different frequency ranges. We note that, for millimeter-wave communication, special attention needs to be paid to hardware impairments and power efficiency, whereas frequency localization is not of great importance.

Table 5.2 Comparison summary of multicarrier waveforms. (Source: mmMAGIC project [4,15])

MC-waveforms	CP-OFDM	W-OFDM	UF-OFDM	FBMC-QAM	FBMC-OQAM
Spectral efficiency	High	High	High	High	High
PAPR	High	High	High	High	High
Phase-noise robustness	Medium	Medium	Low/Medium	Low/Medium	Low/Medium
Robust. to freq. selective chan.	High	High	High/Medium	High	High
Robust. to time-selective chan.	Medium	Medium	Open	Low/Medium	Low/Medium
MIMO compatibility	High	High	Open	Open	Low
Time localization	High	High	High	Low	Low
OOB emissions	High	Medium	Medium	Low	Low
OOB emissions with PA	High	High/Medium	High/Medium	High/Medium	High/Medium
Complexity	Low	Low	Medium	High	High
Flexibility	High	High	High	High	High

5.5 WAVEFORM COMPARISON FOR NR

The mmMAGIC project evaluated several multicarrier and single-carrier waveforms based on the waveform design KPIs discussed in the previous section. The project concluded with an overall comparison of the candidate waveforms prior to the NR standardization in the 3GPP. These results served as an important input for the NR standardization. The waveform comparison results are summarized in Table 5.2 for selected multicarrier waveforms. The following color scheme has been used in this table: Green (light gray in print version) refers to a desirable characteristic; red (medium gray in print version) refers to an undesirable characteristic; blue (dark gray in print version) refers to somewhere between desirable and undesirable characteristic. Moreover, "Open", means that further investigations are required to draw any conclusion. The investigations were based on analytical methods as well as simulations. The simulations were performed under common evaluation assumptions in the mmMAGIC waveform simulators. (One of the two simulators is presented in Chapter 9.) The detailed evaluation results are available in the mmMAGIC project report [4] and are summarized in [15]. In the following, we provide the waveform comparison results for selected KPIs (power efficiency, phase-noise robustness, frequency localization, baseband complexity) and refer the reader to [4] for further details.

5.5.1 FREQUENCY LOCALIZATION

CP-OFDM suffers from poor frequency localization/high out-of-band emissions. Several multicarrier waveforms (both OFDM based and FBMC based) aim at improving frequency localization, as shown in Section 5.1.2 and Section 5.1.3. Among these multicarrier waveforms, FBMC-OQAM ($K = 4$) offers the best frequency localization, followed by FBMC-QAM ($K = 4$), and then UF-OFDM and W-OFDM. However, these waveforms behave differently when they are subject to a realistic power amplifier. For example, under the combination of a high transmission power and moderate to large bandwidths, the spectrum roll-off of all waveforms (W-OFDM, UF-OFDM, FBMC) is similar to CP-OFDM, except very close to band edges where FBMC has a steeper roll-off than W-OFDM and UF-OFDM [4].

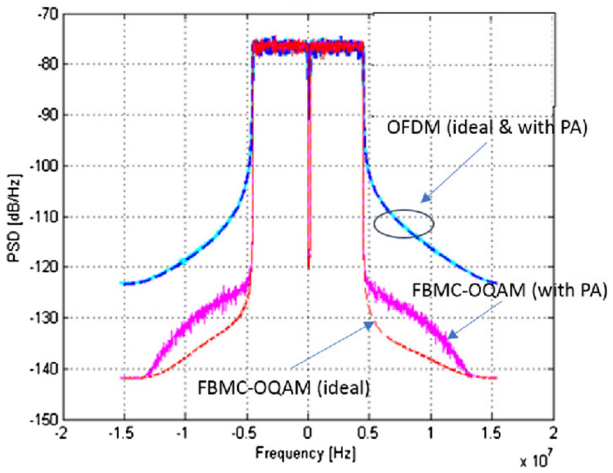

FIGURE 5.33

A PSD comparison of CP-OFDM and FBMC-OQAM with and without PA. Low transmission power and large bandwidth scenario (input power = −21 dBm, output power = 6 dBm, bandwidth = 9 MHz).

In order to show the behavior with respect to nonlinear power amplification, we compare the power spectrum of CP-OFDM and FBMC-OQAM waveforms subject to a power amplifier modeled as a memoryless polynomial in the time domain (as discussed in Chapter 4), according to

$$PA_{output}[n] = PA_{input}[n]p(|PA_{input}[n]|), \tag{5.13}$$

where $p[x] = c_0 + c_1x + c_2x^2 + \cdots + c_kx^k$. For simulations, we have used a tenth order polynomial with coefficients given in [4] and have assumed 2048 subcarriers, 30.72 MHz sampling frequency, and QPSK modulation. For FBMC-OQAM, we have assumed K (overlapping factor) = 4 and the prototype filter given in Table 5.1. In Figs. 5.33–5.35, we compare PSDs of OFDM and FBMC (with and without PA) at different input/output power levels and different signal bandwidths. All PA input/output power values in dBm assume a 50 Ω impedance. We note that the actual transmitter power will be a few (3 to 4) dBs lower due to losses in duplexer/switches. All results are shown without any power back-off. In the following, we summarize the key observations.

- For low transmission power levels or small signal bandwidths, substantially lower OOB emission can be achieved with FBMC compared to OFDM (cf. Fig. 5.33 and Fig. 5.35).
- For high transmission power levels and moderate to high signal bandwidths, the OOB emission is similar for FBMC and OFDM (cf. Fig. 5.35).

In general, for a combination of high transmission power and a large bandwidth, it is unlikely that the sharp spectrum roll-off promised by FBMC and other frequency localized multicarrier waveforms can be realized with state-of-the-art PA technology. In Chapter 8, we provide further evaluations for a power amplifier model with memory.

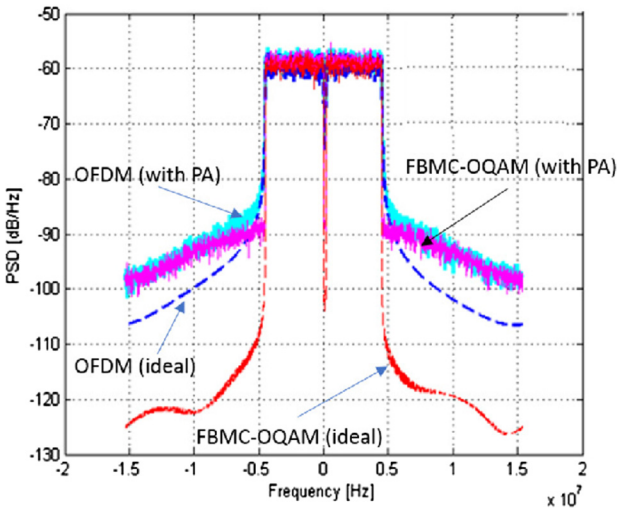

FIGURE 5.34

A PSD comparison of CP-OFDM and FBMC-OQAM with and without PA. High transmission power and large bandwidth scenario (input power = −4 dBm, output power = 24 dBm, bandwidth = 9 MHz).

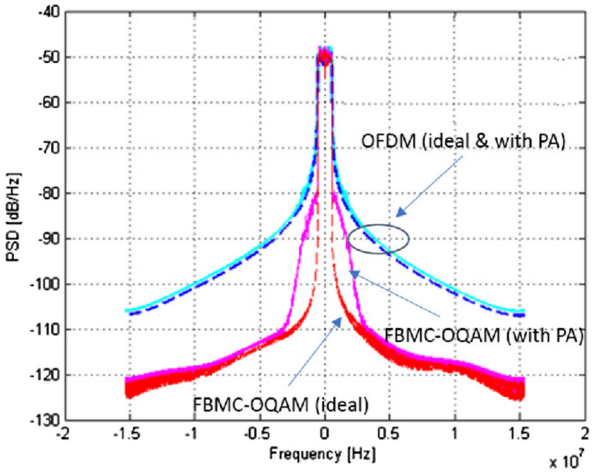

FIGURE 5.35

A PSD comparison of CP-OFDM and FBMC-OQAM with and without PA. High transmission power and small bandwidth scenario (input power = −4 dBm, output power = 24 dBm, bandwidth = 1.08 MHz).

5.5.2 POWER EFFICIENCY

As discussed in Section 5.2, a common drawback of all multicarrier waveforms is their high PAPR (and low power efficiency). In Fig. 5.36, we compare the PAPR of several waveforms, including CP-OFDM,

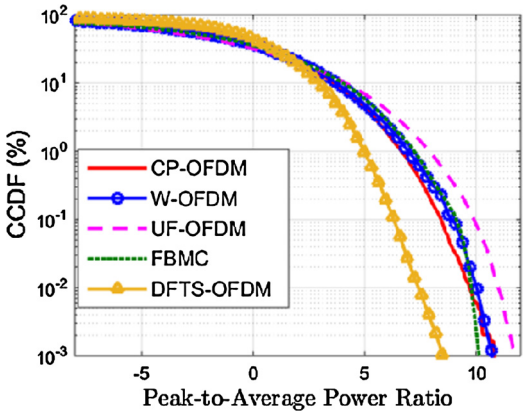

FIGURE 5.36

A comparison of PAPR of multicarrier waveforms and single carrier DFTS-OFDM waveform.

W-OFDM, UF-OFDM, FBMC-OQAM, and DFTS-OFDM (assuming 16 QAM and 1200 subcarriers). We observe that all multicarrier waveforms have similar PAPR except UF-OFDM, which has a higher PAPR. The DFT-based precoding in OFDM (DFTS-OFDM) reduces the PAPR and achieves a higher power efficiency than OFDM. There are various well-known methods to improve the power efficiency of OFDM, which are discussed in Section 6.4.

5.5.3 TIME-VARYING FADING CHANNEL

In Fig. 5.37, we compare performance of several multicarrier waveforms (CP-OFDM, W-OFDM, UF-OFDM, FBMC-OQAM, and FBMC-QAM) in terms of the symbol error rate over a time-varying fading channel with 60 km/h UE speed at 6 GHz carrier frequency (assuming QuaDRiGa channel model). For all waveforms, we assume 16 QAM, 512 subcarriers, and 120 MHz signal bandwidth. As can be seen, CP-OFDM has superior performance in the time-varying fading channel. Further details of this evaluation are given Chapter 9.

5.5.4 BASEBAND COMPLEXITY

We now look at implementation complexity of multicarrier waveforms in terms of the number of real multiplications required for synthesis and demodulation, excluding the computations required for channel estimation. There are different channel estimation techniques used in practice with varying degrees of complexity. We compare complexity of the following multicarrier waveforms: OFDM, W-OFDM, F-OFDM, UF-OFDM, and FBMC. Since FFT/IFFT operations are used in implementations of all of these waveforms, for simplicity we will denote the complexity of an N-point FFT/IFFT operation with $\mathcal{C}_{FFT}(N)$. The results presented in the following are based on [3], where the reader can find a detailed analysis including complexity evaluation for the FPGA-based implementations.

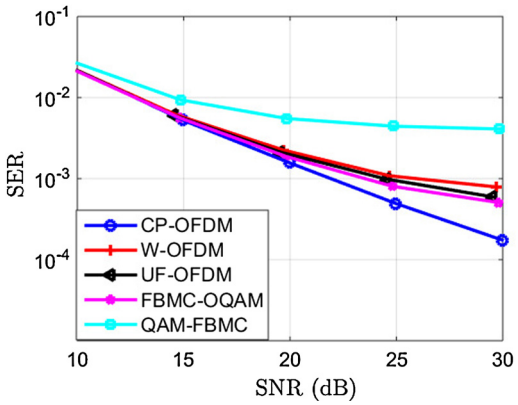

FIGURE 5.37

A comparison of multicarrier waveforms subject to a time-varying fading channel (60 km/h UE speed at 6 GHz carrier frequency).

5.5.4.1 CP-OFDM

Considering the total number of subcarriers N_{sc}, the number of active subcarriers N_{act}, and per subcarrier channel equalization, the number of real multiplications for a CP-OFDM transmitter and receiver are given by

$$\mathcal{C}_{OFDM}^{Tx} = \mathcal{C}_{FFT}(N_{sc}), \tag{5.14}$$

$$\mathcal{C}_{OFDM}^{Rx} = \mathcal{C}_{FFT}(N_{sc}) + 4N_{act}, \tag{5.15}$$

where $4N_{act}$ in (5.15) corresponds to one complex multiplication per subcarrier for channel equalization.

5.5.4.2 W-OFDM

The windowing operation in an OFDM transmitter/receiver is merely multiplication of a window function with an OFDM symbol. Consider an OFDM symbol of length $N_{sc} + N_{cp}$ samples with N_{cp} denoting the number of CP samples, the number of real multiplications for the W-OFDM transmitter and receiver are given by

$$\mathcal{C}_{W-OFDM}^{Tx} = \mathcal{C}_{OFDM}^{Tx} + 4(N_{sc} + N_{cp}) = \mathcal{C}_{FFT}(N_{sc}) + 4(N_{sc} + N_{cp}), \tag{5.16}$$

$$\mathcal{C}_{W-OFDM}^{Rx} = \mathcal{C}_{OFDM}^{Rx} + 4(N_{sc} + N_{cp}) = \mathcal{C}_{FFT}(N_{sc}) + 4N_{act} + 4(N_{sc} + N_{cp}). \tag{5.17}$$

The term $4(N_{sc} + N_{cp})$ corresponds to the number of real multiplications required for the transmitter/receiver windowing operation.

5.5.4.3 UF-OFDM

In the UF-OFDM transmitter, the subcarriers are divided into groups (subbands or resource blocks) and then group-wise filtering is performed. Consider a UF-OFDM symbol with N_{sc} total subcarriers, B groups of N_B subcarriers with group-wise filtering, and a filtering operation in the frequency domain. The number of real multiplications per UF-OFDM symbol is given by

$$\mathcal{C}^{Tx}_{UF-OFDM} = B\left(\mathcal{C}_{FFT}\left(2N_B\right) + \mathcal{C}_{FFT}\left(N_B\right) + 8N_B\right) + \mathcal{C}_{FFT}\left(2N_{sc}\right). \tag{5.18}$$

The UF-OFDM receiver processing includes windowing in the time domain, transformation of the signal to the frequency domain, filtering in the frequency domain, and equalization in the frequency domain. Since the length of a UF-OFDM symbol is $N_{sc} + N_g$ samples (where N_g is the guard interval; cf. Fig. 6.17), the symbol is zero padded and an FFT of size $2N_{sc}$ is performed while we have a transformation from the time to the frequency domain. Considering these operations, the total number of real multiplications is given by

$$\mathcal{C}^{Rx}_{UF-OFDM} = \mathcal{C}_{FFT}(2N_{sc}) + 8N_{sc} + 4N_{act}. \tag{5.19}$$

5.5.4.4 FBMC-OQAM

FBMC waveform can be synthesized via two different approaches: a polyphase network (PPN)-based method and a frequency domain filtering (frequency spread)-based method. The two methods have different implementation complexity. For the PPN implementation, the transmitter and receiver side number of real multiplications (assuming an overlapping factor K for FBMC) are given by

$$\mathcal{C}^{Tx}_{FBMC-PPN} = 2\mathcal{C}_{FFT}(N_{sc}) + 4N_{sc}K + 4N_{act}, \tag{5.20}$$

$$\mathcal{C}^{Rx}_{FBMC-PPN} = 2\mathcal{C}_{FFT}(N_{sc}) + 4N_{sc}K + 4L_{eq}N_{act}, \tag{5.21}$$

where L_{eq} tap channel equalization is performed per subcarrier.

The complexity of the frequency spread FBMC method is given by

$$\mathcal{C}^{Tx}_{FBMC-FS} = 2\mathcal{C}_{FFT}(KN_{sc}) + 8N_{act}(K-1), \tag{5.22}$$

$$\mathcal{C}^{Rx}_{FBMC-FS} = 2\mathcal{C}_{FFT}(KN_{sc}) + 16N_{act}(K-1). \tag{5.23}$$

The transmitter and the receiver side computational complexity of these multicarrier waveforms is compared as a function of the number of subcarriers in Fig. 5.38 and Fig. 5.39, respectively. Here, we have assumed $N_{sc} = N_{act}$ for all waveforms, 7% CP length for OFDM and W-OFDM (i.e., $N_{cp} = .07N_{sc}$), $N_B = 16$ for UF-OFDM, $K = 4$ for FBMC-PPN and FBMC-FS, and $L_{eq} = 3$ for FBMC-PPN. We observe that CP-OFDM has the lowest complexity and the windowing contributes to a minor complexity increase. The complexity of the other multicarrier waveforms is significantly higher than CP-OFDM and the complexity gap enlarges as the number of subcarriers increase. For UF-OFDM, the complexity depends on N_B. As N_B increases, the complexity decreases. We also note that the PPN based FBMC implementation has significantly lower implementation complexity than the frequency spread based implementation.

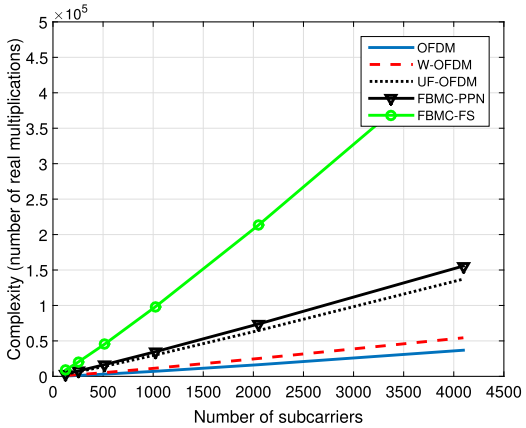

FIGURE 5.38

Transmitter side complexity comparison.

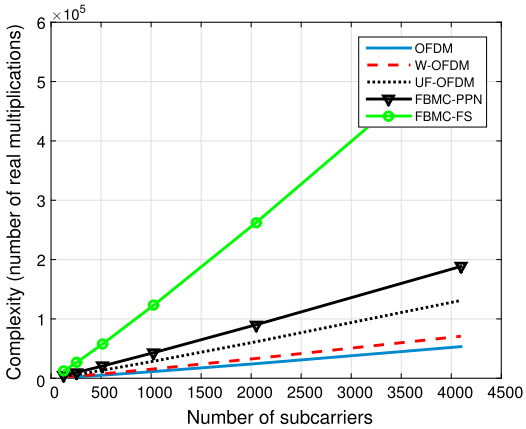

FIGURE 5.39

Receiver side complexity comparison.

5.5.5 PHASE-NOISE ROBUSTNESS COMPARISON

In the following we compare phase-noise robustness of CP-OFDM, FBMC-OQAM, and FBMC-QAM waveforms based on [6]. A baseband signal subject to phase-noise (PN) can be expressed as $r[n] = x[n]\,\mathrm{e}^{j\phi[n]}$, where $\phi[n]$ is a random process. Typically, in a phase-locked loop (PLL)-based oscillators $\phi[n]$ is a wide-sense stationary (WSS) random process, and $|\phi[n]| \ll 1$ [5], which leads to the following approximation:

$$r[n] = x[n]\,\mathrm{e}^{j\phi[n]} \approx x[n](1 + j\phi[n]). \tag{5.24}$$

5.5.5.1 Phase-Noise Effect in OFDM

Assuming that the received OFDM signal $r[n]$ is subject to the PN, consider the demodulation of a subcarrier l in the 0th OFDM symbol (i.e., $s = 0$) without any loss of generality:

$$\begin{aligned} R_{l,0} &= \sum_{n\in\mathbb{Z}} r[n]\,\overline{p_l[n]} \\ &\overset{(a)}{=} \sum_{n\in\mathbb{Z}} \left(\sum_{d\in\mathbb{Z}} \sum_{i\in I} X_{i,d}\; p_i[n-dN] \right) (1 + j\phi[n])\,\overline{p_l[n]} \\ &\overset{(b)}{=} \sum_{i\in I} X_{i,0} \sum_{n\in\mathbb{Z}} p_i[n]\,\overline{p_l[n]}(1 + j\phi[n]) \\ &\overset{(c)}{=} \sum_{i\in I} X_{i,0}\,(\delta_{i,l} + \varphi_{i,l}) \overset{(d)}{=} X_{l,0}\left(1 + \varphi_{l,l}\right) + N_l^{ICI}, \end{aligned} \tag{5.25}$$

where (a) follows from (5.7) and (5.24); (b) follows from the property that consecutive OFDM symbols do not interfere in the time domain ($p_i[n - dN]\,\overline{p_l[n]} = 0\;\forall n \in \mathbb{Z}$ when $d \neq 0$), avoiding intersymbol interference (ISI), (c) follows from $\varphi_{i,l} := \sum_{n\in\mathbb{Z}} j\,\phi[n]\,p_i[n]\,\overline{p_l[n]}$ and $\sum_{n\in\mathbb{Z}} p_i[n]\,\overline{p_l[n]} = \delta_{i,l}$, where $\delta_{i,l}$ is the Kronecker delta function; (d) follows by defining $N_l^{ICI} := \sum_{i\in I_{ICI}} X_{i,0}\,\varphi_{i,l}$, and $I_{ICI} = I \setminus \{l\}$ is the set of subcarriers that interfere with subcarrier l due to the PN. According to (5.25), the transmitted symbol X_l is multiplied by the term $(1 + \varphi_{l,l})$. This effect is known as a common phase error (CPE) because it causes an identical phase rotation in all subcarriers (i.e., $\varphi_{l,l} = \varphi_{k,k}$ for any l, k). The additive term N_l^{ICI} refers to an intercarrier interference (ICI), which is different for different subcarriers (that is, $N_l^{ICI} \neq N_k^{ICI}$ for any $l \neq k$).

According to [6], the achievable signal-to-interference ratio (SIR) of the demodulated subcarrier l in the OFDM symbol subject to the PN (in absence of CPE) is given by

$$\mathrm{SIR}_l = \frac{1}{\left(\int_{-0.5}^{+0.5} S_\phi(\nu)\; W_l^{ICI}(\nu)\, d\nu \right)}, \tag{5.26}$$

where

$$W_l^{ICI}(\nu) := \sum_{i\in I_{ICI}} \frac{1}{N^2} \left| \frac{\sin\left(\pi\left(\nu - \frac{i-l}{N}\right) N\right)}{\sin\left(\pi\left(\nu - \frac{i-l}{N}\right)\right)} \right|^2. \tag{5.27}$$

Next, we evaluate the achievable SIR using (5.26) for the PLL based phase-noise model described in Section 4.2.3. The PSDs of the PN model are illustrated in Fig. 5.40 at three oscillator different frequencies: 6 GHz, 28 GHz, and 82 GHz. The achievable SIR as a function of the subcarrier spacing is shown in Fig. 5.41. We observe that the SIR is an increasing function of the subcarrier spacing. This implies that the OFDM system would be more robustness against the PN if a larger subcarrier spacing is used.

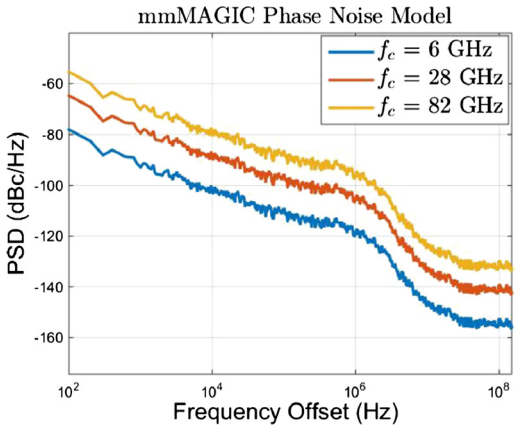

FIGURE 5.40

Power spectrum of the PLL based PN model at three oscillator frequencies: 6 GHz, 28 GHz, and 82 GHz. The model is developed in mmMAGIC (a European research project).

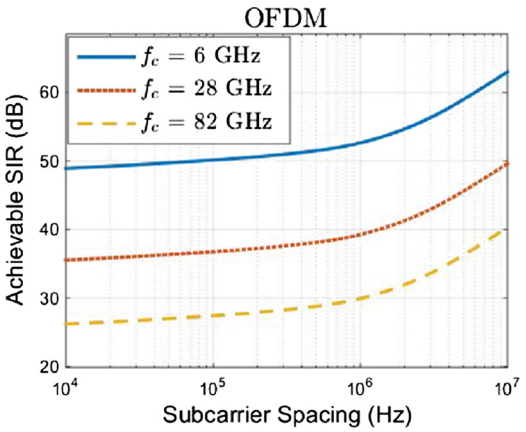

FIGURE 5.41

Achievable signal-to-interference ratio (SIR) for OFDM as a function of its subcarrier spacing at three oscillator frequencies (6 GHz, 28 GHz, and 82 GHz).

5.5.5.2 Phase-Noise Effect in FBMC-QAM

The demodulation of a subcarrier l in the 0th FBMC-QAM symbol (i.e., $s = 0$) subject to the PN is given by

$$R_{l,0} = \sum_{n \in \mathbb{Z}} r[n] \, \overline{p_l[n]}$$

$$\begin{aligned}
&\overset{(a)}{=} \sum_{n\in\mathbb{Z}} \left(\sum_{d\in D} \sum_{i\in I} X_{i,d}\; p_i[n-dN] \right) (1+j\phi[n])\; \overline{p_l[n]} \\
&= \sum_{d\in D} \sum_{i\in I} X_{i,d} \sum_{n\in\mathbb{Z}} p_i[n-dN]\; \overline{p_l[n]}\; (1+j\phi[n]) \\
&\overset{(b)}{=} \sum_{d\in D} \sum_{i\in I} X_{i,d} \left(\lambda_{i,l,d} + \beta_{i,l,d} \right),
\end{aligned} \tag{5.28}$$

where (a) follows from (5.24) and (5.11) and (b) follows by defining

$$\lambda_{i,l,d} := \sum_{n\in\mathbb{Z}} p_i[n-dN]\; \overline{p_l[n]}\,, \tag{5.29}$$

$$\beta_{i,l,d} := \sum_{n\in\mathbb{Z}} j\phi[n]\; p_i[n-dN]\; \overline{p_l[n]}\,. \tag{5.30}$$

The term $\lambda_{i,l,d}$ is due to the self-interference components caused by the overlapping FBMC symbols and the nonorthogonality between the subcarriers, whereas $\beta_{i,l,d}$ is due to the PN; it depends on both the choice of the prototype filters and the PN. We can rewrite (5.28) as

$$R_{l,0} = X_{l,0} \left(1+\beta_{l,l,0}\right) + I_l^{ICI} + I_l^{ISI} + N_l^{ICI} + N_l^{ISI}, \tag{5.31}$$

where we have used the following notations:

$$I_l^{ICI} := \sum_{i\in I_{ICI}} X_{i,0}\, \lambda_{i,l,0}\,, \tag{5.32}$$

$$I_l^{ISI} := \sum_{d\in D_{ISI}} \sum_{i\in I} X_{i,d}\, \lambda_{i,l,d}\,, \tag{5.33}$$

$$N_l^{ICI} := \sum_{i\in I_{ICI}} X_{i,0}\, \beta_{i,l,0}\,, \tag{5.34}$$

$$N_l^{ISI} := \sum_{d\in D_{ISI}} \sum_{i\in I} X_{i,d}\, \beta_{i,l,d}\,, \tag{5.35}$$

where $D_{ISI} = D \setminus \{0\}$ is a set containing the indices of the FBMC-QAM symbols that overlap with the 0th FBMC-QAM symbol. The multiplicative term $(1+\beta_{l,l,0})$ corresponds to the CPE. The CPE has the same value for all even subcarriers and the same value for all odd subcarriers (i.e., $\beta_{k,k,0} = \beta_{l,l,0}$ if $k \bmod 2 = l \bmod 2$ for any l,k). The terms I_l^{ICI} and I_l^{ISI} model the ICI and the ISI due to the self-interferences and the terms N_l^{ICI} and N_l^{ISI} represent the ICI and the ISI due to the PN.

According to [6], the achievable SIR of the demodulated subcarrier l in the FBMC-QAM symbol subject to the PN (in absence of CPE) is given by

$$\mathrm{SIR}_l = \frac{P_X}{P_{I_l^{ICI}} + P_{I_l^{ISI}} + P_{N_l^{ICI}} + P_{N_l^{ISI}}}, \tag{5.36}$$

$$P_{N_l^{ICI}} := P_X \left(\int_{-0.5}^{+0.5} S_\phi(\nu)\, W_l^{ICI}(\nu)\, d\nu \right), \tag{5.37}$$

$$P_{N_l^{ISI}} := P_X \left(\int_{-0.5}^{+0.5} S_\phi(\nu)\, W_l^{ISI}(\nu)\, d\nu \right), \tag{5.38}$$

$$P_{I_l^{ICI}} := P_X\, \delta(\nu)\, W_l^{S-ICI}(\nu), \tag{5.39}$$

$$P_{I_l^{ISI}} := P_X\, \delta(\nu)\, W_l^{S-ISI}(\nu), \tag{5.40}$$

$$W_l^{ICI}(\nu) := \sum_{i \in I_{ICI}} W_{i,l,0}(\nu), \tag{5.41}$$

$$W_l^{ISI}(\nu) := \sum_{d \in D_{ISI}} \sum_{i \in I} W_{i,l,d}(\nu), \tag{5.42}$$

$$W_l^{S-ICI}(\nu) := \sum_{i \in I_{ICI}} W_{i,l,0}^{S}(\nu), \tag{5.43}$$

$$W_l^{S-ISI}(\nu) := \sum_{d \in D_{ISI}} \sum_{i \in I} W_{i,l,d}^{S}(\nu), \tag{5.44}$$

$$W_{i,l,d}(\nu) := W_{i,l,d}^{S}(\nu) = \left| P_i(\nu)\, e^{-j2\pi\nu dN} \circledast \overline{P_l(\nu)} \right|^2, \tag{5.45}$$

where $P_i(\nu) := \mathcal{F}\{p_i[n]\}$, $p_i[n]$ is defined in (5.12), and $\mathcal{F}\{\cdot\}$ is the discrete-time Fourier transform operation.

5.5.5.3 Phase-Noise Effect in FBMC-OQAM

Assuming that the received FBMC-OQAM signal $r[n]$ is subject to the PN, the demodulation of a subcarrier l in the 0th FBMC-OQAM symbol is given by:

$$\begin{aligned}
R_{l,0} &\overset{(a)}{=} \sum_{n \in \mathbb{Z}} \Re r[n]\, \psi_l\, \overline{p_l[n]} \\
&\overset{(b)}{=} \sum_{n \in \mathbb{Z}} \Re \left\{ \left(\sum_{d \in D} \sum_{i \in I} X_{i,d} \theta_{i,d}\, p_i \left[n - d\frac{N}{2} \right] \right) (1 + j\phi[n])\, \psi_l\, \overline{p_l[n]} \right\} \\
&= \sum_{d \in D} \sum_{i \in I} X_{i,d} \sum_{n \in \mathbb{Z}} \Re \left\{ \theta_{i,d}\, p_i \left[n - d\frac{N}{2} \right] \psi_l\, \overline{p_l[n]}\, (1 + j\phi[n]) \right\} \\
&\overset{(c)}{=} \sum_{d \in D} \sum_{i \in I} X_{i,d} \left(\gamma_{i,l,d} + \rho_{i,l,d} \right)
\end{aligned}$$

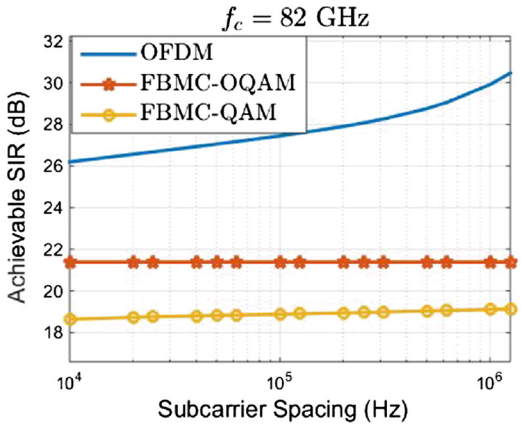

FIGURE 5.42

Achievable signal-to-interference ratio (SIR) for OFDM, FBMC-OQAM ($K = 4$) and FBMC-QAM ($K = 4$) as a function of subcarrier spacing at 82 GHz oscillator frequency.

$$\stackrel{(d)}{=} X_{l,0} + I_l^{ICI} + I_l^{ISI} + N_l^{ICI} + N_l^{ISI}, \tag{5.46}$$

where (a) follows from the offset-demapping which uses the real value operator $\Re\{\cdot\}$ and the phase term $\psi_l = j^{(-l)}$; (b) follows from (5.24) and (5.10); (c) follows by defining

$$\gamma_{i,l,d} := \sum_{n\in\mathbb{Z}} \Re\left\{\theta_{i,d}\; p_i\left[n - d\frac{N}{2}\right]\psi_l\;\overline{p_l[n]}\right\}, \tag{5.47}$$

$$\rho_{i,l,d} := \sum_{n\in\mathbb{Z}} \Re\left\{j\phi[n]\,\theta_{i,d}\; p_i\left[n - d\frac{N}{2}\right]\psi_l\;\overline{p_l[n]}\right\}, \tag{5.48}$$

which are associated with the self-interferences and the PN, respectively; (d) follows from defining I_l^{ICI}, I_l^{ISI} (the same as in (5.32) and (5.33) but replacing $\lambda_{i,l,d}$ by $\gamma_{i,l,d}$), N_l^{ICI} and N_l^{ISI} (the same as in (5.34) and (5.35), but replacing $\beta_{i,l,d}$ by $\rho_{i,l,d}$). It is noteworthy that FBMC-OQAM is not affected by any CPE effect subject to the given PN formulation (i.e., $\forall l \in I\ \rho_{l,l,0} = 0$).

According to [6], the achievable SIR of the demodulated subcarrier l in the FBMC-OQAM symbol subject to the PN is given by (5.36) with the following differences:

$$W_{i,l,d}(\nu) := \frac{1}{4}\left[\left|V_d\left(\nu - \frac{i-l}{N}\right)\right|^2 + \left|V_d\left(\nu + \frac{i-l}{N}\right)\right|^2 - \right.$$
$$\left. - 2\,\Re Y_{i,l,d}(\nu)\right] \tag{5.49}$$

$$W^S_{i,l,d}(\nu) := \frac{1}{4}\left[\left|V_d\left(\nu - \frac{i-l}{N}\right)\right|^2 + \left|V_d\left(\nu + \frac{i-l}{N}\right)\right|^2 + \right.$$
$$\left. + 2\,\Re Y_{i,l,d}(\nu)\right], \tag{5.50}$$

where $Y_{i,l,d}(\nu) := e^{j\pi(i-l+d)} V_d\left(\nu - \frac{i-l}{N}\right) V_d^*\left(\nu + \frac{i-l}{N}\right)$, $V_d(\nu) := P(\nu) \circledast \left(P(\nu)e^{-2\pi\nu\frac{N}{2}d}\right)$, and $P(\nu) := \mathcal{F}\{p[n]\}$.

In Fig. 5.42, we compare the achievable SIRs for OFDM, FBMC-OQAM ($K = 4$), and FBMC-QAM ($K = 4$) as functions of the subcarrier spacing at 82 GHz oscillator frequency. We observe that the FBMC waveforms are more sensitive to phase noise than OFDM.

REFERENCES

[1] M. Bellanger, FS-FBMC: an alternative scheme for filter bank based multicarrier transmission, in: 5th International Symposium on Communications Control and Signal Processing (ISCCSP), 2012, May, pp. 1–4.

[2] M. Bellanger, et al., FBMC physical layer: a primer, http://www.ict-phydyas.org, 2010, 06.

[3] R. Gerzaguet, N. Bartzoudis, L.G. Baltar, V. Berg, J.B. Doré, D. Kténas, O. Font-Bach, X. Mestre, M. Payaró, M. Färber, K. Roth, The 5G candidate waveform race: a comparison of complexity and performance, EURASIP Journal on Wireless Communications and Networking 2017 (1) (2017, Jan.).

[4] J. Luo, A.A. Zaidi, J. Vihriälä, D. Giustiniano, et al., Preliminary radio interface concepts for mm-wave mobile communications. Deliverable D4.1, Millimetre-Wave Based Mobile Radio Access Network for Fifth Generation Integrated Communications (mmMAGIC), https://5g-mmmagic.eu/results, 2016.

[5] A. Mehrotra, Noise analysis of phase-locked loops, in: IEEE/ACM International Conference on Computer Aided Design. ICCAD – 2000. IEEE/ACM Digest of Technical Papers (Cat. No.00CH37140), 2000, Nov., pp. 277–282.

[6] V. Moles-Cases, A.A. Zaidi, X. Chen, T.J. Oechtering, R. Baldemair, A comparison of OFDM, QAM-FBMC, and OQAM-FBMC waveforms subject to phase noise, in: 2017 IEEE International Conference on Communications (ICC), 2017, May, pp. 1–6.

[7] H.G. Myung, J. Lim, D.J. Goodman, Single carrier fdma for uplink wireless transmission, IEEE Vehicular Technology Magazine (ISSN 1556-6072) 1 (3) (2006, Sept.) 30–38, https://doi.org/10.1109/MVT.2006.307304.

[8] H. Nam, M. Choi, C. Kim, D. Hong, S. Choi, A new filter-bank multicarrier system for QAM signal transmission and reception, in: Proc. IEEE ICC, 2014, June, pp. 5227–5232.

[9] F. Schaich, T. Wild, Y. Chen, Waveform contenders for 5G—suitability for short packet and low latency transmissions, in: IEEE Vehicular Technology Conference (VTC Spring), 2014, May, pp. 1–5.

[10] F. Sjoberg, R. Nilsson, M. Isaksson, P. Odling, P.O. Borjesson, Asynchronous zipper, in: IEEE International Conference on Communications (ICC), 1999, pp. 231–235.

[11] T. Wild, F. Schaich, A reduced complexity transmitter for UF-OFDM, in: Proc. IEEE 81st Vehicular Technology Conference (VTC Spring), 2015, May, pp. 1–6.

[12] T. Wild, F. Schaich, Y. Chen, 5G air interface design based on universal filtered (UF-)OFDM, in: 19th International Conference on Digital Signal Processing (DSP), 2014, Aug., pp. 699–704.

[13] Y.H. Yun, C. Kim, K. Kim, Z. Ho, B. Lee, J.Y. Seol, A new waveform enabling enhanced QAM-FBMC systems, in: Proc. IEEE SPAWC, 2015, June, pp. 116–120.

[14] A.A. Zaidi, R. Baldemair, H. Tullberg, H. Bjorkegren, L. Sundstrom, J. Medbo, C. Kilinc, I.D. Silva, Waveform and numerology to support 5G services and requirements, IEEE Communications Magazine (ISSN 0163-6804) 54 (11) (2016, November) 90–98, https://doi.org/10.1109/MCOM.2016.1600336CM.

[15] A.A. Zaidi, J. Luo, R. Gerzaguet, H. Wang, X. Chen, Y. Qi, N. Cassiau, A. Wolfgang, J. Vihriala, A. Kakkavas, T. Svensson, J. Mohammadi, R.J. Weiler, M. Dieudonne, H. Halbauer, V. Moles-Cases, H. Miao, Evaluation of waveforms for mobile radio communications above 6 GHz, in: 2016 IEEE Globecom Workshops (GC Wkshps), 2016, Dec., pp. 1–6.

[16] L. Zhang, A. Ijaz, P. Xiao, M.M. Molu, R. Tafazolli, Filtered OFDM systems, algorithms, and performance analysis for 5G and beyond, IEEE Transactions on Communications (ISSN 0090-6778) 66 (3) (2018, March) 1205–1218, https://doi.org/10.1109/TCOMM.2017.2771242.